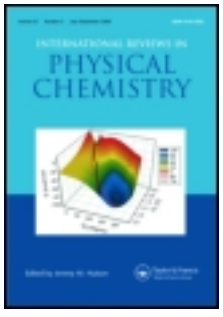

International Reviews in Physical Chemistry

Publication details, including instructions for authors and subscription information:
http://www.tandfonline.com/loi/trpc20

# Ultrafast equilibrium and non-equilibrium chemical reaction dynamics probed with multidimensional infrared spectroscopy

Jessica M. Anna [a], Carlos R. Baiz [a], Matthew R. Ross [a], Robert McCanne [a] & Kevin J. Kubarych [a]

[a] Department of Chemistry, University of Michigan, Ann Arbor, MI 48109, USA

Version of record first published: 28 Sep 2012.

To cite this article: Jessica M. Anna, Carlos R. Baiz, Matthew R. Ross, Robert McCanne & Kevin J. Kubarych (2012): Ultrafast equilibrium and non-equilibrium chemical reaction dynamics probed with multidimensional infrared spectroscopy, International Reviews in Physical Chemistry, DOI:10.1080/0144235X.2012.716610

To link to this article: http://dx.doi.org/10.1080/0144235X.2012.716610

*International Reviews in Physical Chemistry*
2012, 1–53, iFirst



# Ultrafast equilibrium and non-equilibrium chemical reaction dynamics probed with multidimensional infrared spectroscopy

Jessica M. Anna, Carlos R. Baiz, Matthew R. Ross, Robert McCanne and Kevin J. Kubarych*

*Department of Chemistry, University of Michigan, Ann Arbor, MI 48109, USA*

(*Received 11 June 2012; final version received 25 July 2012*)

Two-dimensional infrared (2D-IR) spectroscopy provides powerful tools to investigate chemical reaction dynamics in the condensed phase. Correlating excitation and detection frequencies grants access to structural and dynamical information that is hidden in a linear absorption spectrum. Low-barrier reactions naturally can occur on the picosecond time scale, and although they are too rapid to study using nuclear magnetic resonance spectroscopy, the intrinsic ultrafast time resolution of coherent 2D-IR spectroscopy enables direct tracking of equilibrium reactive barrier crossings. 2D-IR chemical exchange spectroscopy can monitor the picosecond dynamics of non-triggered chemical reactions by correlating excited reactant frequencies with detected product frequencies. Solvent and temperature-dependent variations enable comparisons with microscopic rate theories at an unprecedented level of detail. 2D-IR spectroscopy is also emerging as a powerful probe of non-equilibrium light-driven chemical transformations. Transient 2D-IR spectroscopy is able to follow nascent photoproducts caused by electronic excitation or by a temperature jump. Soon it will be possible to study transient species with the full range of 2D observables, such as line shapes and waiting-time dynamics that have motivated the wide adoption of equilibrium 2D-IR spectroscopy. This review summarises the general progress in using 2D-IR spectroscopy to study chemical reactions in solution, focusing on our investigations into reactions of isomerisation of $CO_2(CO)_8$, photodissociation of $Mn_2(CO)_{10}$, geminate rebinding in $[CpMo(CO)_3]_2$ and charge transfer in betaine-30 as viewed from the first solvation shell.

**Keywords:** multidimensional spectroscopy; reaction dynamics; activated barrier crossing; photolysis; geminate rebinding; solvation dynamics; charge transfer



**Contents**



*Corresponding author. Email: kubarych@umich.edu

ISSN 0144–235X print/ISSN 1366–591X online

http://dx.doi.org/10.1080/0144235X.2012.716610
http://www.tandfonline.com

## 1. Introduction

A central goal of research in physical chemistry is to watch chemical reactions and dynamics as they happen. The most direct approaches would track the making and breaking of chemical bonds and the transfer of energy and charge with the highest possible time resolution while simultaneously recording molecular motions. In the condensed phase, such details can be challenging to extract due to the complexity of interactions with the environment and the fast time scales associated with fundamental chemical events. Ultrafast spectroscopy certainly provides access to transient femtosecond and picosecond phenomena, and with the advent of multidimensional extensions in the infrared (IR), visible and even UV, we are now witnessing qualitative improvements in spectral resolving power while sacrificing little time resolution.

From the perspective of chemical reaction dynamics, it is possible, at least operationally, to separate transformations into equilibrium and non-equilibrium reactions. Here, we refer to an equilibrium reaction as one that is unsynchronised and requires no external trigger, relying solely upon random thermal fluctuations to proceed from reactants to products. This is precisely the class of reactions that we denote with a double-headed arrow in undergraduate chemistry textbooks. Traditionally, these processes have been difficult to study on ultrafast time scales, where most spectroscopic techniques exploit a trigger – typically a laser pulse – to initiate a photochemical reaction, such as an excited

electronic state isomerisation reaction. Indeed, the vast majority of ultrafast studies of chemical reactions have been photoinitiated non-equilibrium processes.

Using two-dimensional infrared (2D-IR) spectroscopy, it is now possible to investigate the dynamics of both equilibrium and non-equilibrium chemical reactions. Equilibrium reactions lead to time-dependent changes in the 2D-IR spectrum due to the random exchange of reactants and products [1–3]. Provided a spectroscopic signature of the stable species exists, it is generally possible to extract exchange rate constants directly from 2D spectra. Combined with equilibrium constants, it is straightforward to deduce the forward and reverse rate constants. It is then tempting to use the temperature dependence of the rate constant to perform an Arrhenius analysis, yielding the energy barriers [4,5]. However, as we discuss below, such an approach can lead to difficulties, particularly in the diffusive regime where solvent friction not only modulates the barrier crossing, but also has a non-trivial temperature dependence. Nevertheless, considerable progress has been made in applying so-called 2D-IR 'chemical exchange' spectroscopy to a wide range of systems including hydrogen bond making and breaking [3,6–13], complexation reactions [3,12,14,15], isomerisation [5,16,17], and Berry pseudo-rotation [4].

Provided one manages to achieve sufficient sensitivity, it is possible to use 2D spectroscopy as a non-equilibrium probe of transient chemical processes [18–20]. By simply inserting a photochemically or photophysically active pulse (an 'actinic' pulse) either before or within the 2D-IR sequence, the transient 2D spectrum can reveal details of the transient species that are either impossible or difficult to infer from traditional transient IR absorption spectroscopy. These experiments were introduced by Hamm and have since found some degree of adoption in the broader 2D community, though they remain technically challenging. In addition to the extensive work on photoswitchable peptides [18,21–24], there are now several examples of photodissociation [25–30], geminate rebinding [31], charge transfer [32] and temperature jumps [33,34]. In principle, any system that has been successfully studied with transient IR absorption could be studied with transient 2D-IR, with the caveat that in general the signal-to-noise ratio will be much smaller.

2D-IR spectroscopy enables the design of experiments that push the limits of conventional assumptions and approximations, revealing aspects of dynamics that can only be treated by speculation using 1D spectroscopy. By studying reactions, either at equilibrium or driven by light, we access regions of the potential energy surface where there is necessarily a tight interplay between electronic and nuclear degrees of freedom. Having the most powerful spectroscopic tool available is essential to a detailed understanding of the reacting system, its internal degrees of freedom and how those are coupled to the environment. In the following section, we describe some of the recent progress in addressing the key challenges in chemical reaction dynamics using 2D-IR spectroscopy.

## 2. Multidimensional IR spectroscopy

Multidimensional optical spectroscopy has gained popularity in recent years, thanks to several technological and conceptual developments including the recasting of somewhat esoteric perturbation theory and quantum dissipation into more or less familiar chemical concepts. There are now several accessible reviews [35–45], tutorials [46] and

monographs [47,48] that provide varying levels of details for those entering the field. We summarise here the key aspects of 2D-IR spectroscopy that are relevant to the discussion of the applications reviewed below.

### 2.1. *2D-IR spectroscopy: practicalities*

2D-IR spectroscopy is a third-order non-linear technique where three external IR pulses induce a response in a material that leads to the generation of a signal whose field is detected either in the time or in the frequency domains. In practice, the mid-IR (1000–4000 $cm^{-1}$) pulses are generated by non-linear frequency conversion of pulses from a near-IR laser system based on a Ti:sapphire chirped-pulse amplifier centred at 800 nm. Multistage parametric amplification results in μJ-level pulses in the mid-IR with typical durations less than 100 fs. Commercial optical parametric amplification (OPA) systems have been available for many years; a typical OPA requires a minimum of 0.25–0.5 mJ of input pulse energy (assuming a 1 kHz amplifier system) [49].

In a sense, a 2D-IR spectrum is a pump–probe transient absorption spectrum with equal spectral resolution of the pump and the probe, with the added feature that the two frequencies are correlated. That is, the amplitude at any point in the $\omega_{excite}$–$\omega_{detect}$ grid reports the probability of detecting signal at $\omega_{detect}$ given excitation at $\omega_{excite}$. Based on this starting point, there are two basic ways to implement 2D spectroscopy. Historically, the first method involves the scanning of a relatively narrow band pump pulse through the absorption spectrum of the sample (Figure 1), while recording the transient absorption of a broad-band probe pulse [50]. There are several ways to generate the narrow-band pump, including a low-finesse scanning Fabry–Pérot interferometer or a dispersive pulse shaper based either on a scanned slit [51] or a programmable acousto-optic modulator [52]. More recently, a particular broad-band method has been implemented by Bian *et al*. [53], where a relatively narrow band picosecond pulse is generated by a picosecond Ti : sapphire laser system pumping an OPA; a second femtosecond laser system generates the broad-band mid-IR probe. Methods that employ a hybrid frequency–time-domain approach derive their excitation frequency resolution from the bandwidth of the pump pulse, and due to the nature of the Fourier transform (FT) relationship between frequency- and time-domain fields, a high frequency resolution is necessarily accompanied by lower time resolution.

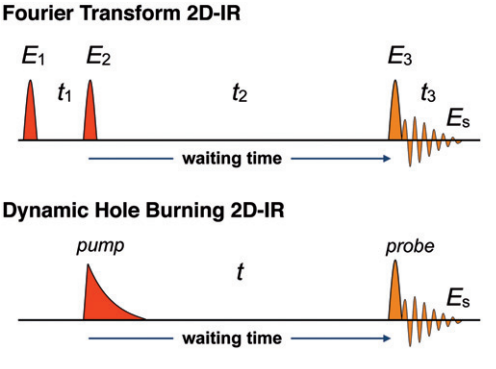


Figure 1. (Colour online) Pulse sequences for FT (top) and dynamic hole burning (bottom) 2D-IR spectroscopy.

Nevertheless, for many practical molecular systems in the IR, one can find a suitable compromise between time and frequency resolution [54].

The alternative to a tuneable pump pulse is a pair of pulses whose relative time delay is scanned, yielding an FT 2D spectrum (Figure 1) [55]. This approach provides the best combination of time and frequency resolution, but one is generally required to produce the full spectral bandwidth needed for the experiment in a single pulse, or using two pulses centred at different frequencies [56–58]. It is also essential to maintain interferometric stability, or to reliably measure the pulse-pair delay to a precision much better than the mid-IR oscillation period. This method is the most commonly implemented, but it is also the least intuitive, so we will focus our discussion here on the FT implementation of 2D-IR spectroscopy.

The pulse sequence for a three-pulse FT 2D spectrum is shown in Figure 1. The three fields are denoted $E_1$, $E_2$ and $E_3$, with wavevectors $\mathbf{k_1}$, $\mathbf{k_2}$ and $\mathbf{k_3}$, arriving at times 0, $t_1$ and $t_1 + t_2$, respectively. Following the usual perturbation theory approach, to third order in the applied fields, there are eight possible output signals with wavevectors $\mathbf{k_s} = \pm\mathbf{k_1} \pm \mathbf{k_2} \pm \mathbf{k_3}$, and by arranging the three incident pulses on the corners of a square (or equivalently an equilateral triangle), the four-wave mixing signal $\mathbf{k}_- = -\mathbf{k_1} + \mathbf{k_2} + \mathbf{k_3}$ can be isolated spatially. By swapping the arrival times of the first two pulses, a different signal will emerge in the same location at the $\mathbf{k}_-$ signal; we denote this signal as $\mathbf{k}_+ = +\mathbf{k_1} - \mathbf{k_2} + \mathbf{k_3}$, where the sign refers to the sign of $\mathbf{k_1}$ in each sequence. These two signals are referred to as the 'rephasing' ($\mathbf{k}_-$) and 'non-rephasing' ($\mathbf{k}_+$) signals; the terminology is justified below.

It is not sufficient to record the intensity of the emitted signal, since it would not yield the 2D spectrum following Fourier transformation with respect to $t_1$. Instead, we must detect the electric field of the signal, which requires an interferometric measurement [59]. In the fully non-collinear implementation, the solution is to use spectral interferometry by introducing a fourth external pulse derived from $E_3$ [60]. Spectral interferometry is a method that allows the determination of the spectral phase difference between a reference field – often denoted a 'local oscillator' – and a signal field. The addition of another interference requires control or knowledge of the optical path length at a level that is substantially smaller than the wavelength of light. In the IR, it is straightforward to maintain phase stability between two fields that travel on different optical paths, and so it is common for the local oscillator field to bypass the sample before being combined with the signal field in the spectrometer (or, alternatively, the time-domain interferometer) for spectral detection. In some cases, particularly for temperature-jump measurements of protein folding, it is actually helpful to send the local oscillator through the sample in order for it to experience the same phase shifts as the signal field [33].

With the signal field available from spectral interferometry, all that remains is to scan the $t_1$ delay. Unfortunately, this step can be the most difficult aspect of recording a 2D spectrum. Most translation stages equipped with roof mirrors or corner cubes will introduce some slight amplitude and beam-pointing fluctuations, often oscillatory, which when the signal is Fourier transformed, appear as artefacts such as side bands. To circumvent the reflective delay, several groups have implemented movable wedge pairs, where by scanning one wedge with respect to the other, the optical path length of the combined pair changes and imparts an exceptionally controllable time delay [61]. In the mid-IR, ZnSe is a nearly ideal material; it has a high index of refraction, but low dispersion. Hence a 7° apex ZnSe

wedge pair can produce time delays up to 12 ps with 25 mm of translation. Using optical encoders with ~7 nm resolution, one can easily and reproducibly change time delays at the sub-wavelength level [62].

Since there is no requirement that the first two pulses be non-collinear, it is possible to implement 2D-IR spectroscopy in a 'pump–probe'' geometry. The simplest method uses one output channel of a Mach–Zehnder interferometer to produce the two excitation pulses, while the other output channel serves to monitor the interferometer [63]. An alternative approach is to use a mid-IR pulse shaper based on a 4-f design, where a germanium acousto-optic modulator acts in the Fourier plane to generate controllable phase masks capable of producing the requisite pump pulse pair [64–67]. Here, the time delay is essentially perfectly known, and other pulse phase modulations can be applied to remove scatter and reproduce signals that are measured using the fully non-collinear geometry. In both of these partially collinear schemes, the probe acts as the local oscillator and interferometric stability is automatically maintained between the signal and the local oscillator since they are co-propagating.



### 2.2. *Chirped-pulse upconversion*

Spectral detection poses a technical challenge to implementing 2D-IR spectroscopy, and limits its use in laboratories not dedicated to transient IR spectroscopy. Though it is quite common to use array detectors in the visible, such as efficient and relatively inexpensive CCD cameras, in the mid-IR, array detectors are comparably expensive, with narrower spectral coverage and fewer pixels. An alternative that we have found to be very effective is to convert the mid-IR signal back into the visible using sum frequency generation with a highly chirped 800 nm pulse, where detection is easily achieved using a thermoelectrically cooled CCD camera (Roper PIXIS) [62,68–72]. This camera provides 1340 horizontal pixels and can be programmed to operate at a 1 kHz repetition rate. Although mixing the non-linear signal and the local oscillator with a chirped pulse causes some cross-phase modulation, the effect is easily reversed by a simple, one-time measurement of the chirped pulse's time-dependent instantaneous frequency (or, equivalently its spectral phase) followed by a simple correction procedure [62,69]. Very recently, a promising material, $AgGaGeS_4$, has been shown to extend upconversion of mid-IR pulses into the range 1000–1800 $cm^{-1}$ while not sacrificing the range up to 3000 $cm^{-1}$ that is already possible using $LiNbO_4$ [73].

### 2.3. *2D-IR: chemical information*

#### 2.3.1. *Coupling and spectral assignments*

The information contained in a 2D-IR spectrum can be generally divided into two categories: structure and dynamics. Vibrational spectra are, in principle, always sensitive to and determined by molecular structure since different functional groups are generally characterised by somewhat distinct spectral bands. In practice, it is exceptionally rare that a synthetic chemist would use an IR spectrum to determine a structure, though IR bands can support an assignment. Molecular vibrations are often regarded as corresponding to the normal modes, though these are necessarily based on a harmonic approximation, and the true vibrational eigenstates are actually anharmonic and coupled. In any case, it is

straightforward to show that a purely harmonic model, coupled or not, will not give rise to a non-linear response function [74]. Hence, 2D-IR spectroscopy is particularly useful for exposing the network of vibrational coupling that results from the anharmonic nuclear Hamiltonian. Recent work by Bian *et al.* [53], for example, illustrates nicely the full information content available, provided one is able to record a 2D spectrum over the remarkably broad band of frequencies from 1000 to 3000 $cm^{-1}$. The coupling between modes is encoded in the amplitude of vibrational cross peaks that appear between two diagonal peaks in the 2D spectrum as well as in their polarisation dependence.

In dilute solutions, where intermolecular energy transfer is unlikely, cross peaks can only be observed between modes on the same molecule (or species of molecule). Cross peaks can therefore be used to assign IR spectra, particularly when multiple species are present either because of an intentional mixture of different molecules [75] or an equilibrium distribution of different stable isomers [5,17,76].



### 2.3.2. *Intramolecular vibrational redistribution*

Besides the instantaneous cross peaks present at short waiting times ($t_2$) that reflect the coupling directly in the nuclear Hamiltonian, vibrational energy redistribution among eigenstates with similar energies also adds amplitude to cross peaks in 2D-IR spectra. Intramolecular vibrational redistribution (IVR) serves to statistically scramble the state-selective excitation in a 2D spectrum. The time scales for IVR can vary widely from sub-picoseconds to many tens of picoseconds or longer, at which point most systems will have fully vibrationally relaxed, thus limiting the accessible temporal dynamic range. IVR is particularly difficult to generalise since there are many examples in the literature showing pronounced state and solvent dependencies, which can render energy matching and spatial overlap pictures only marginally useful. Still, significant progress by Rubtsov [43] and Lin and Rubtsov [77] has been made in using IVR to provide distance information from the perspective of so-called 'relaxation-assisted 2D-IR'. In metal carbonyl systems, where sharp vibrational resonances often lie well within $k_BT$ of each other, IVR has been used to sense solvent-specific solvation exposing non-monotonic hydrogen bonding when compared with atomistic molecular dynamics (MD) simulations [78]. Changes in IVR time scales determined using transient 2D-IR show that before and after photolysis of hydrogenase model compounds' vibrational redistribution is structurally specific [29,51,79]. It is also worth mentioning that since transitions among different pairs of vibrational eigenstates are often polarised differently, IVR can appear in transient absorption anisotropy measurements. Both IVR and the IVR-associated anisotropy decay have analogies in ultrafast electronic spectroscopy, where, for example, it is quite common to use transient absorption anisotropy to study ultrafast energy transfer.

### 2.3.3. *Orientational relaxation*

Since experiments use polarised light, both diagonal and cross peaks in a 2D-IR spectrum include a dynamical orientational factor that depends on the waiting time. Initially photoselected molecules orientationally diffuse in solution, leading to a general decay in the 2D signal. In a pump–probe experiment, it is possible to measure (or isolate by combining separate measurements) the isotropic response function by arranging the polarisations between the pump and probe pulses at the magic angle of 54.7° where the

orientational component of the orientationally averaged signal vanishes. Since a 2D spectrum is recorded with a sequence of three pulses, by recording separately the tensor elements $R^{(3)}_{xxxx}$ and $R^{(3)}_{xxyy}$, their combination yields the isotropic response $R^{(3)}_{iso}$ [80]:

$$R^{(3)}_{iso} = \frac{R^{(3)}_{xxxx} + 2R^{(3)}_{xxyy}}{3} \tag{1}$$

Alternatively, it is possible to simply record the isotropic response with $E_3$ polarised at 54.7° relative to $E_1$ and $E_2$, provided one has a way to phase the spectrum, or by using an implementation that has no phase uncertainty [81]. Similarly, the anisotropic response $R^{(3)}_{aniso}$ can be constructed from the same tensor elements:

$$R^{(3)}_{aniso} = \frac{R^{(3)}_{xxxx} - R^{(3)}_{xxyy}}{R^{(3)}_{xxxx} + 2R^{(3)}_{xxyy}} = \frac{R^{(3)}_{xxxx} - R^{(3)}_{xxyy}}{3R^{(3)}_{iso}} \tag{2}$$

The anisotropic 2D spectra of water have been reported by both Ramasesha *et al*. [80] and Hamm *et al*. and they illustrate that the inhomogeneously broadened OH stretching band also displays frequency-dependent (and therefore hydrogen bond length dependent) orientational relaxation time scales [82]. In many systems studied with 2D-IR, such as peptides and proteins, or smaller molecules in hydrogen bonding solvents, the molecular reorientation times are much longer than the vibrational lifetimes, which simplifies the analysis of waiting-time-dependent measurements.

### 2.3.4. *Spectral diffusion*

In the condensed phase, optical spectra are broadened by interactions with the surroundings. The solvent – which could be a simple liquid or a protein, membrane surface, etc. – may act to cause frequency fluctuations in a probed solute. Ideally, one would measure these frequency trajectories directly, and thus extract all possible dynamical information about the solute. In practice, it is not possible, even with single-molecule techniques, to record such a trajectory. Instead, using non-linear spectroscopy, one may measure quantities that are proportional to time correlation functions of the frequency fluctuations [74]. It is essential to note that in what follows we tacitly assume that the act of performing spectroscopy on a subset of a solute's degrees of freedom does not influence the dynamics of either the solute or the solvent. Such a simplifying assumption is not always warranted, as has been seen clearly in experimental [83–85] and theoretical [86,87] studies of methanol, where vibrational excitation of the hydroxyl OD stretch induces OD $\cdots$ O bond rupture.

Since a 2D spectrum correlates an excited and a detected frequency, any inhomogeneous frequency memory that persists beyond the homogeneous dephasing time will give rise to a diagonally elongated 2D line shape (Figure 2). For a static system, this line-shape asymmetry will remain for all waiting times, but in solution at least the partial loss of frequency correlation results from environmental fluctuations. To reliably deduce the time scale for spectral diffusion, it is necessary to record both the rephasing and the non-rephasing signals, which are often combined into an absorptive spectrum by setting the relative phase between the two 2D spectra using a somewhat independent pump–probe spectrum [88]. Alternatively, measurements recorded in a pump–probe geometry – either using a Mach–Zehnder interferometer, a pulse shaper or a spectral filter – directly yield absorptive 2D spectra. In the fully non-collinear beam geometry, which can have

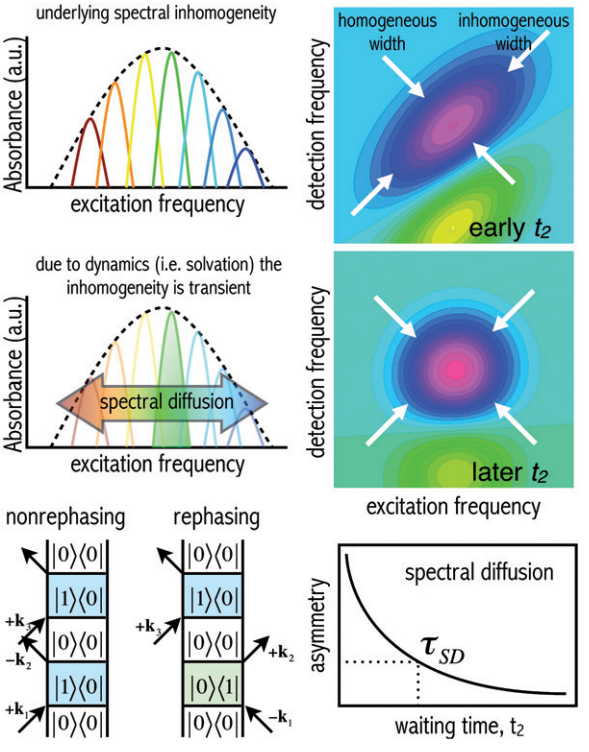


Figure 2. (Colour online) Spectral diffusion that is directly observable using 2D-IR spectroscopy. (top) Distinct microscopic environments within an inhomogeneously broadened band lead to diagonally elongated 2D spectra at early waiting times. (middle) As the ensemble stochastically samples these microscopic environments, frequency correlation is lost, resulting in a symmetric line shape at later waiting times. (bottom) Feynman diagrams for a two-level system corresponding to non-rephasing and rephasing pathways illustrate the phase conjugation (or lack thereof) responsible for the echo in the rephasing pathway. Time resolving the loss of correlation yields a time scale for spectral diffusion.

sensitivity advantages over the pump–probe implementations, the phasing process is often cumbersome, particularly when one wishes to record hundreds of 2D spectra under different experimental conditions of solvent or temperature. To circumvent the phasing process and avoid recording a pump–probe spectrum, it is possible to extract the spectral diffusion by using the absolute value 2D rephasing ($A_R$) and non-rephasing ($A_N$) spectra alone. By numerically comparing the two pathways, it is possible to extract all the homogeneous components and leave only the 'echo' contribution. The ability of a system to rephase and produce the echo will necessarily decay as the oscillators find themselves in different environments characterised by different vibrational transition frequencies. Such stochastic frequency changes cannot be reversed by a sequence of optical pulses, and the echo amplitude decays with increased waiting time. Roberts *et al.* [89] introduced the so-called inhomogeneity index $I_{inh}$ as:

$$I_{inh} = \frac{A_R - A_N}{A_R + A_N} \tag{3}$$

and showed that it is proportional to the time correlation function of the frequency fluctuations under only very mild assumptions. Since the two absolute value spectra should be equal after the spectral diffusion is complete, the inhomogeneity index can be thought of as a normalised measure of equilibrium solvation, in much the same way that non-equilibrium solvation progress is reported in time-dependent Stokes' shift measurements [90]. The inhomogeneity index dramatically simplifies the task of extracting spectral diffusion from 2D-IR spectra and may make it possible to record spectral diffusion of, for example, quasi-equilibrated excited electronic state vibrations using transient 2D spectroscopy.



#### 2.3.5. *Chemical exchange*

When there are two or more species present in equilibrium that are separated by a small energetic barrier (<10 kcal/mol), it may be possible to observe dynamic interconversions provided there is some spectral signature unique to the various species and that the vibrational lifetime is long enough to capture the dynamics. Chemical exchange can be viewed as an example of spectral diffusion among well-defined microscopically distinct subensembles (i.e. a reactant and a product) separated by energy barriers. Molecules initially excited in one conformation will stochastically sample all available conformations, and the probability of having exchanged during the waiting time $t_2$ is determined by the solution to a phenomenological rate equation. Because of the ultrafast nature of 2D-IR and the necessity for low barriers due to the finite vibrational lifetime, it is possible that non-exponential kinetics may be observed [91], reflecting the finite transit time from a reactant well to the transition state (TS). Though such a time-dependent rate 'constant' has been predicted in a simple model of a double-well system, to date there have not been any experimental observations of the effect using 2D-IR spectroscopy. Chemical exchange is described in greater detail in Section 3.

### 2.4. *Transient 2D-IR*

Transient methods bring the powerful information available from 2D spectroscopy to non-equilibrium species. Many of the limitations of linear, ID spectroscopy are present in transient 1D ultrafast spectroscopy. These include the inability to separate inhomogeneous and homogeneous contributions to transient line shapes. Transient 2D-IR methods, though still quite challenging, have nevertheless been applied to a wide range of condensed phase systems. The basic implementation is conceptually simple: one merely needs to add another pulse to the sequence that either prepares a non-equilibrium initial condition or abruptly alters the system as it evolves during the waiting time of the 2D-IR sequence (Figure 3). The first type of experiment is denoted 'pump–probe' transient 2D-IR, or sometimes simply t-2D-IR. 18,19,24]. A pump–probe t-2D-IR experiment can be viewed either as an effective, difference third-order measurement or as a fifth-order measurement. Since most implementations published in the literature use a single additional pump with wavevector $\mathbf{k}_{trig}$, the transient signal propagates in the same direction as the equilibrium signal because the fifth-order signal wavevector is given by either

$$\mathbf{k}_R^{(5)} = \left(-\mathbf{k}_{trig} + \mathbf{k}_{trig}\right) - \mathbf{k}_1 + \mathbf{k}_2 + \mathbf{k}_3 \tag{4}$$

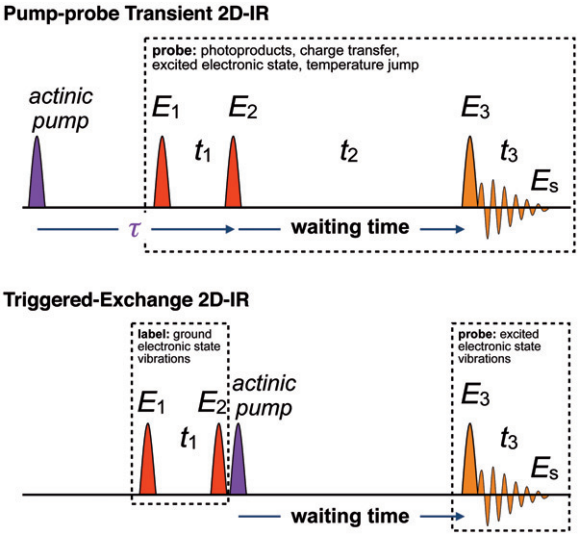


Figure 3. (Colour online) Pulse sequences for pump–probe transient (top) and triggered-exchange (bottom) 2D-IR spectroscopy.

for the transient rephasing signal or by

$$\mathbf{k}_N^{(5)} = \left(-\mathbf{k}_{trig} + \mathbf{k}_{trig}\right) + \mathbf{k}_1 - \mathbf{k}_2 + \mathbf{k}_3 \tag{5}$$

for the transient non-rephasing signal. It is possible to use two non-collinear trigger beams to produce a background-free transient signal, though such an implementation has not yet been achieved experimentally in fifth-order experiments with mixed frequency domains. In 2D Raman or 3D-IR, however, fully non-collinear geometries have been used, producing background-free signals which can be heterodyne detected using a reference local oscillator [92–94]. For transient 2D-IR spectroscopy, it is relatively straightforward to align the spatial and temporal overlap of the actinic trigger by monitoring the modulation of the four-wave mixing echo signal.

Another pulse sequence, denoted 'triggered-exchange', orders the actinic pump within the 2D-IR sequence (Figure 3) [26,95,96]. Here, the goal is to correlate vibrations between different electronic Hamiltonians. For example, in the case of a molecule that is electronically excited, it should be possible to map the vibrational modes of the ground state to those of the excited state, effectively projecting the excited-state vibrations onto the basis of the ground state, which can be known to a high accuracy using quantum chemical calculations. One inevitable limitation of triggered-exchange 2D-IR is the presence of IVR, which may scramble the vibrational labels before the trigger pulse arrives. Also, non-equilibrium solvation dynamics launched by the electronic excitation can also serve to enhance IVR on the excited state, effectively erasing the correlation with the initially excited ground electronic state vibrations. It should also be possible to implement triggered-exchange 2D-IR in the non-collinear actinic pump geometry, which could be very helpful in removing the often overlapping ground electronic state 2D-IR bleach that can obscure transient spectra. Double-sided Feynman diagrams for the two

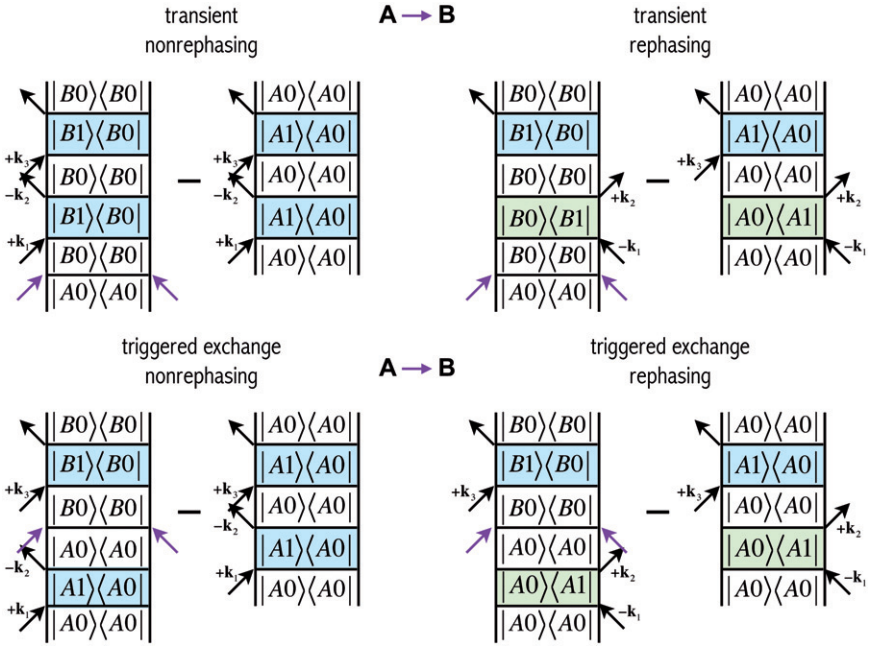


Figure 4. (Colour online) Double-sided Feynman diagrams for the non-equilibrium 2D-IR pulse sequences for a hypothetical photochemical or photophysical processes where absorption of a photon of an actinic pulse (represented by the two coincident, unlabeled field interactions) induces a change from system A to system B. For simplicity, excited vibrational state pathways and those where the trigger pulse excite vibrations are not shown. The signal can be computed by subtracting the triggered and untriggered 2D spectra.

types of transient pulse sequences are shown in Figure 4. Since only a fraction of molecules are electronically excited by the actinic pump, it is necessary to compute the difference 2D spectrum.

### 2.5. *Transient dispersed vibrational echo*

It is not always practical to record a transient 2D spectrum due to the Draconian demands on signal-to-noise ratios. As a method that lies partway between transient IR absorption and transient 2D-IR, transient dispersed vibrational echo (DVE) enables some of the benefits of a non-linear probe without introducing debilitating complications [97,98]. For fixed $t_1$ and $t_2$ delays, the four-wave mixing signal emitted from the sample can be detected either with heterodyne detection or directly as an intensity. If the sample has some spectral inhomogeneity, then a non-zero $t_1$ will actually cause a larger signal for the rephasing sequence due to the generation of the photon echo. Historically, the time delay at which one finds the maximum echo signal is called the echo 'peak shift' and forms the basis for three-pulse echo peak shift spectroscopy. In a transient DVE experiment, shown in Figure 5, the whole sequence of three pulses acts as the probe of a transient process, providing good signal-to-noise ratios due to the background-free nature of the beam geometry, though clearly with lower time resolution than would be achieved with a single

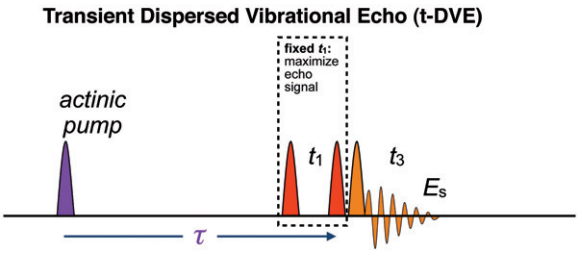


Figure 5. (Colour online) Pulse sequence for transient DVE spectroscopy.



IR probe pulse. An in-depth comparison of transient DVE and transient IR absorption shows that as long as the detection method is the same, the transient DVE signal will yield a greater signal-to-noise ratio [97]. For cases where one seeks primarily information about kinetics, without requiring the highest time or frequency resolution, transient DVE spectra can be quite informative. Further, at low bleach levels the non-heterodyne-detected transient DVE signal is practically proportional to the number of molecules excited, rather than the square as would be expected for an intensity-detected non-linear signal. It is also possible to introduce a local oscillator for heterodyne detection of the complex echo field, from which the homodyne-detected echo can be recovered with spectral interferometry [98].

## 3. Equilibrium reaction dynamics: chemical exchange

### 3.1. *Basic principles of 2D-IR chemical exchange*

At equilibrium, although there are no macroscopic changes, chemical reactions nevertheless continue with, on average, an equal number of forward and reverse reactions per unit time. For reactions with large barriers, it is straightforward to follow the reaction kinetics by mixing species in an initially non-equilibrium ratio of reactants and products, and monitoring the mixture in real time until the reaction 'stops,' at which point it has re-established an equilibrium. For low-barrier reactions ($E_a < 20$ kcal/mol), the time scale for re-equilibration is too fast to track in real time using even the fastest chemical mixing devices. To determine the kinetics for low-barrier reactions, one requires ultrafast chemical probes of equilibrium phenomena. To understand how 2D-IR spectroscopy provides a solution, we consider two species (denoted I and II) in equilibrium separated by a TS (denoted ‡), as depicted in Figure 6. Assuming well-separated vibrational transitions characteristic of the two species, centred at $\omega_I$ and $\omega_{II}$ a 2D-IR spectrum at waiting times much shorter than the reaction time will contain only two peaks (ignoring any other transitions as well as all excited-state absorption). This initial 2D spectrum can be viewed as having an inhomogeneous broadening consisting of two principal subensembles. With increased waiting time, some molecules initially excited as species I at $\omega_I$ may isomerise to species II and emit at $\omega_{II}$ resulting in a cross peak. The waiting-time dependence of this exchange cross peak reveals the underlying kinetics. From the spectral inhomogeneity perspective, the evolution of the exchange peak is a special case of spectral diffusion in the presence of a barrier (or diffusion in a force field). Indeed, this diffusion picture is precisely what motivates the theory, due to Kramers, of activated barrier crossings in the

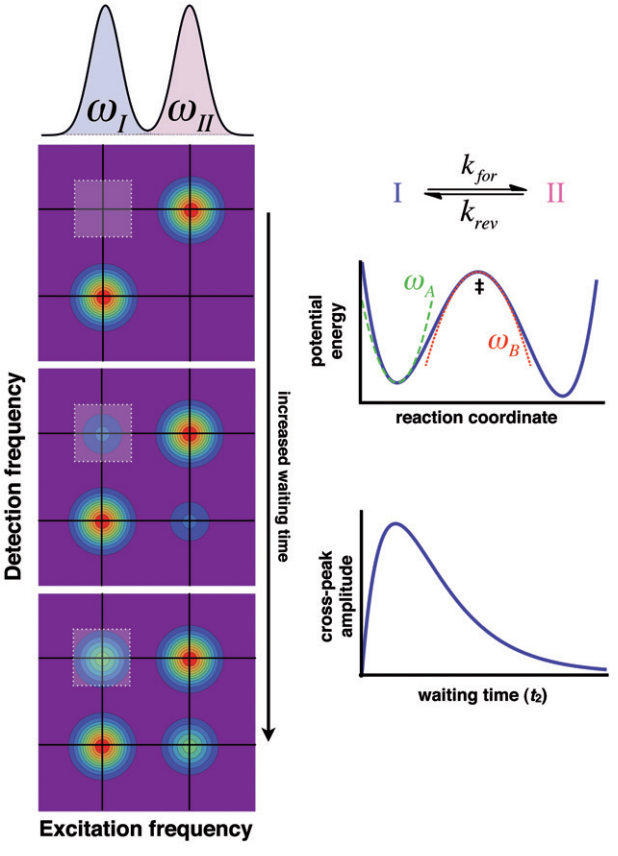


Figure 6. (Colour online) Ultrafast chemical exchange between two species (I and II) with characteristic IR transitions at $\omega_I$ and $\omega_{II}$. (left) With increased waiting times, cross peaks appear between the two bands indicating that some molecules, initially excited as on species, were found to have exchanged at the given waiting time. (right) A simple two-state kinetic scheme and a corresponding 1D reaction surface with harmonic fits to the stable basin and TS (‡) correspond to the derivation in the text. By monitoring the cross-peak amplitude as a function of waiting time, it is possible to extract the exchange rate constant.

condensed phase. Between the limiting cases of idealised two-state exchange and a truly continuous ensemble, one may imagine an intermediate regime of tens or hundreds of important conformations that interconvert with small barriers, such as what one might expect within a macromolecule such as a protein. In large complex systems, one would expect heterogeneities in both the barriers and the dynamical friction, leading to non-exponential kinetics, similar to what we have observed in a glass-forming liquid [99].

The first transient IR experiments that reported the equilibrium making and breaking of hydrogen bonds between triethylsilanol and acetonitrile were denoted ‘tag and probe’ by Arrivo *et al*. [100] and Arrivo and Heilweil [101]. In these experiments, a relatively narrow band pulse excites either the higher frequency free OH of the silanol, or the lower frequency hydrogen-bonded complex with acetonitrile, followed by a narrow-band probe

of the $v = 1$–2 excited-state absorption of either the free or bound species. Clearly, in currently terminology, this information is identical to what would be measured in a 2D-IR chemical exchange experiment, albeit from only two points of the full 2D surface. Since these two points contain much of the information that would be extracted from a full 2D-IR measurement at multiple waiting times, this early work should be regarded as the first IR implementation of chemical exchange spectroscopy, and the authors reported a lifetime of $70 \pm 15$ ps for the hydrogen bonded complex.

Early 2D-IR experiments that explicitly attributed spectral dynamics to chemical exchange (and hence making the analogy with nuclear magnetic resonance (NMR) spectroscopy) were reported by Woutersen *et al.* [102], where two distinct conformations of *n*-methyl acetamide in methanol were observed to interconvert on a time scale shorter than the amide-I vibrational lifetime. In this case, the formation of a hydrogen bond with methanol red shifts the amide-I carbonyl stretch relative to the non-hydrogen-bonded carbonyl. This slight spectral difference is sufficient to track the making and breaking of hydrogen bonds with the prototypical protein backbone unit.

The key observable quantity that emerges from a chemical exchange experiment is the exchange rate constant. Assuming a two-state kinetic scheme (Figure 6), the instantaneous concentration of one species $c_A(t)$ can be described by the following [103]:

$$c_A(t) = \langle c_A \rangle + \delta c_A(t) \tag{6}$$

where $\langle c_A \rangle$ is the equilibrium concentration and $\delta c_A(t)$ the instantaneous deviation from equilibrium caused by random thermal fluctuations that lead to barrier crossings. The time dependence of the deviation is often deduced from phenomenological chemical kinetics to be

$$\delta c_A(t) = \delta c_A(0) e^{-k_{exch} t} \tag{7}$$

by solving the rate equations for a two-species system, where $k_{exch} = k_{for} + k_{rev}$. That is, the system will relax towards equilibrium with an observed rate constant given by the sum of the forward and reverse reaction rate constants. This relaxation is simply a manifestation of the Onsager regression hypothesis underlying linear response theory. The parameter of interest – the exchange rate constant – can in principle be measured either using a system at equilibrium or one perturbed away from equilibrium, provided linear response still holds.

For reactions probed with 2D-IR exchange spectroscopy, the first-order approximation is that the optical excitation does not affect the underlying chemical dynamics. Hence, though the system is clearly not at equilibrium with respect to the spectroscopic degree of freedom, all other degrees of freedom remain at equilibrium, and the coupling between them is assumed (or known) to be weak. There are, however, several examples of cases where IR excitation can lead to real chemical bond breaking, such as the dissociation of hydrogen bonds in methanol [83]. Assuming that the dynamics associated with the low-barrier, ultrafast reactive crossing remains at equilibrium, what, then, is out of equilibrium and thus visible with spectroscopy? By exciting molecules of a given species type, and not of another type, which is effectively possible using non-linear spectroscopy, our knowledge of which molecules were initially excited is momentarily out of equilibrium. As the molecules interconvert stochastically, we lose our ability to correlate an excited and detected molecule. Experimentally, this return to equilibrium of our vibrational excitation

tag leads to a growth in a cross peak at the location of a coincidence of the product and the reactant vibrational transition. We note that it should be possible to observe chemical exchange even when there are no clearly resolvable exchange cross peaks, but where the overall inhomogeneously broadened band is composed of contributions from chemically distinct species. There, the chemical exchange would be responsible for spectral diffusion, and one may choose to classify this regime as the 'fast-exchange' or the nearly fast-exchange regime. One example of this type of exchange has been found in the intramolecular rotational isomerisation of ethyl isocyanate using the conformational sensitivity of the N=C=O stretch as revealed by temperature-dependent dephasing times [104].

Because of the requirement that the barrier-crossing processes must occur while some reasonable fraction of molecules is still vibrationally excited, there are fundamental limitations on both the barrier heights and equilibrium constants (or effective populations) that can be studied with 2D exchange spectroscopy. Here, we introduce the term 'effective population' since it is possible for different species to have different transition strengths. Using a particularly simple kinetic model that includes only two reacting species and vibrational energy relaxation, we have shown that the maximum exchange signal amplitude is given by the following expression [76]:

$$S_{\max} = \frac{B_0 k_{for}}{k_{vib}} \left( \frac{k_{sum}}{k_{vib}} \right)^{-\left( \frac{k_{sum}}{k_{for}+k_{rev}} \right)} \tag{8}$$

where $k_{sum} = k_{for} + k_{rev} + k_{vib}$ $B_0$ is the initial effective population and $k_{vib}$ is the vibrational relaxation rate constant (i.e. $1/T_1$). In general, we take the initial effective population to equal the amplitude of a diagonal peak corresponding to a given species. From this expression, it is possible to estimate the experimental signal-to-noise ratio required to measure an exchange cross peak in a realistic 2D spectrum. This expression is, however, only an estimate since no vibrational energy transfer – due to IVR – has been included.

### 3.2. *Examples: unimolecular and bimolecular reactions*

Chemical exchange has a long history in NMR spectroscopy, where it is possible to observe reactions occurring over a wide range of time scales [105]. In NMR, it is common to set a time scale for the so-called 'fast exchange' between two species (with chemical shifts $\delta_A$ and $\delta_B$ in frequency units) such that interconversion is more rapid than the inverse of the chemical shift difference. In the IR, however, the range is limited to very low barrier processes, typically <10 kcal/mol, because of the finite lifetime, as discussed in the previous section. Following the first report of hydrogen bond exchange by Woutersen *et al.* [102], both Zheng *et al.* [12] and Kim and Hochstrasser [11] reported complexation and hydrogen bond breaking, respectively. These experiments were the first to explicitly borrow the language and analytical approach from NMR chemical exchange and apply it to ultrafast 2D-IR measurements. Zheng *et al.* [15] followed their studies of the complexed-to-free reaction of phenol and benzene in chloroform with a series of studies varying phenol substituents. They were also able to use exchange to watch hydrogen bond rearrangements in ionic solutions [106,107], and at interfaces [108–110], as well as the rotation about a C–C

single bond [16]. In a biochemical setting, they leveraged the conformational sensitivity of the CO stretch frequency in a mutant of myoglobin to track the exchange of population between different conformational substates of a globular protein [111]. In addition to several examples in small molecules and peptides [2,11,112–115], Ghosh *et al.* [116] invoked a chemical exchange picture to explain observations made within the M2 proton channel of the influenza A virus. As a proton arrived or departed from a nearby histidine residue, it induces a dramatic shift in the local electrostatic environment, leading to a significant spectral fluctuation, which is sensed by the spectral diffusion of a nearby probe chromophore, in this case an isotopically labelled backbone amide carbonyl.

In addition to several hydrogen bond rearrangement processes – at ionic solutes and within supramolecular complexes, for example – there have been some examples of unimolecular reactions involving the motion of several atoms to cross a well-defined TS. One such example is the observation of cross-peak growth in $Fe(CO)_5$ (iron pentacarbonyl, IPC) attributed to vibrational energy mixing induced by the geometrical distortion associated with Berry pseudo-rotation [117,118]. The NMR observation of a single $^{13}C$ peak even at the lowest possible temperatures indicated that fast, fluxional motions led to the scrambling of the carbonyl ligands, swapping axial and equatorial carbonyl units on a time scale of picoseconds [119]. Using 2D-IR spectroscopy, Cahoon *et al.* [4] were able to time resolve the fluxional reaction and used temperature dependence to extract a reaction barrier that was consistent with the $\sim$2 kcal/mol value computed using density functional theory for a $C_{4v}$ TS.

The justification of the specific form of the TS, which is the one proposed by Cotton [118], is achieved by mapping the overlap of the CO displacements of vibrational eigenmodes in the stable basin with those in the TS. Since the minimum energy configuration of IPC is trigonal bipyramidal ($D_{3h}$), the IR active vibrations partition into two bands, one doubly degenerate ($e'$ symmetry) centred at 1999 $cm^{-1}$, and one ($a_2''$ symmetry) at 2022 $cm^{-1}$. These modes share no common local carbonyl units, and therefore, despite their very small energy difference, vibrational energy transfer between the modes should be highly improbable, especially in the weakly interacting non-polar *n*-dodecane solvent.

Though the primary goal of the IPC study was to show that the 2D-IR measurements were consistent with the structure of the TS, the Arrhenius analysis points to another role that ultrafast chemical exchange can play in investigating the fundamental physical chemistry of activated processes. The viscosities of solvents are temperature dependent, so for low-barrier reactions which might be in or near the diffusion-limited regime, changing temperature can also affect the observed rate constant due to altered solvent friction. Indeed, for reactions with barriers on the $<$5 kcal/mol level, the Arrhenius-law solvent viscosity can contribute an effective 'barrier' that is comparable to the solvent-free barrier. For example, in the case of *n*-dodecane used in the IPC study, the viscosity decreases by a factor of two, from 1.344 to 0.659 cP, over the temperature range from 25° to 75°C. If a reaction's rate constant were inversely proportional to the solvent viscosity, as found in some simple models using Kramers' theory, the temperature-dependent viscosity alone would appear as a barrier of 2.8 kcal/mol. Therefore, using any temperature dependence to extract activation barriers for ultrafast reactions requires care, attention must be paid to the role of the surrounding environment in modulating the reactive crossings. The summary of our approach to this key issue will comprise the subject of the remainder of this section.

### 3.3. *Chemical exchange as a test of Kramers' theory*

The starting point for a detailed understanding of chemical kinetics is transition state theory (TST), which is a non-dynamical description of the likelihood of visiting an activated complex assuming purely equilibrium thermodynamics. Whether formulated from the perspective of statistics, thermodynamics or even microscopic molecular trajectories, one finds that there is essentially no requirement to ever consider the influence of the environment except through its purely energetic contribution to the reaction-free energy surface [103]. The dynamic route to derive TST, which is based on the time-correlation function of the reactive flux through the barrier, leads to the important realisation that the very existence of a rate constant presupposes that all the dynamics associated with traversing the barrier occur on a distinct time scale from the fundamental ultrafast molecular relaxation. It is worth noting that for low-barrier processes, the solvation dynamics a molecule experiences within a stable basin can occur on time scales that are quite similar to those associated with the barrier crossing itself.

#### 3.3.1. *Kramers' theory background*

Kramers' theory emerges from a stochastic description of a diffusive particle in one dimension ($x$) with mass $m$, subject to a potential $V(x)$, a velocity-dependent friction $\zeta$ and a random fluctuating force $A(t)$:

$$m\ddot{x}(t) = -\frac{\mathrm{d}V(x)}{\mathrm{d}x} - \zeta\dot{x}(t) + A(t) \tag{9}$$

Kramers solved this equation in various limits, finding essentially two regimes: the energy-controlled regime where increased friction aids reactive crossings by supplying the molecule with thermal excitation and a diffusion-controlled regime where added friction induces more recrossings of the barrier. Between these two regimes, there is a turnover which defines the maximum rate constant. In the diffusion-controlled regime, the expression for the rate constant is:

$$k_{Kramers} = \frac{1}{\omega_b}\frac{\beta}{2}\left\{\left[1 + \left(\frac{2\omega_b}{\beta}\right)^2\right]^{1/2} - 1\right\}k_{1\mathrm{DTST}} = Fk_{1\mathrm{DTST}} \tag{10}$$

where $k_{1\mathrm{DTST}}$ is the ID TST rate constant, $\omega_b$ is the second-order curvature of the barrier; $\beta$ is unitless and proportional to the friction and $E_a$ is the activation barrier [120].

The 1D TST rate constant is given by

$$k_{1\mathrm{DTST}} = \frac{k_B T}{h}\frac{Q^*}{Q_A}e^{-\frac{E_a}{k_B T}} \tag{11}$$

where $Q^*$ and $Q_A$ are the partition functions of the TS and reactant basin, respectively. For a 1D reaction, $Q^*$ is equal to unity since the TS has zero degrees of freedom. Using a harmonic approximation for the reactant potential with frequency, $\omega_A$, $Q_A$ becomes:

$$Q_A = \frac{1}{1 - \exp\left[\frac{H_A}{k_B T}\right]} \approx \frac{1}{1 - \exp\left[\frac{\hbar\omega_A}{k_B T}\right]} \tag{12}$$

where $H_A$ is the Hamiltonian of the reactant basin. Expanding the exponential term in a power series results in the following:

$$\exp\left[\frac{\hbar\omega_A}{k_BT}\right] = 1 + \frac{\hbar\omega_A}{k_BT} + \cdots \tag{13}$$

Combining Equations (12) and (13) and making use of the fact that $Q^* = 1$, the ratio of the partition functions is

$$\frac{Q^*}{Q_A} = \frac{\hbar\omega_A}{k_BT} \tag{14}$$

Substituting Equation (14) into the expression for $k_{\mathrm{TST}}$ (Equation (11)) results in the expression for $k_{1\mathrm{DTST}}$ [121]:

$$k_{1\mathrm{DTST}} = \frac{k_BT}{h}\left(\frac{h\omega_A}{2\pi k_BT}\right)e^{-\frac{E_a}{k_BT}} = \frac{\omega_A}{2\pi}e^{-\frac{E_a}{k_BT}} \tag{15}$$

Thus, the Kramers result can be thought of as a correction to TST where the variable $F$ in Equation (10) takes into account the influence of the solvent on the barrier-crossing process. There exist extensions to basic TST, where the influence of a bath can be incorporated effectively, leading to a minimised path from reactants to products. This so-called variational TST is an elegant theoretical formulation that, though highly successful, lacks the simplicity of a more modular approach that results from Kramers' analysis of stochastic motion on an energy surface [122–125].

By considering the so-called reduced rate constant defined as [126]:

$$k_{red} = k_{exp}\exp\left(\frac{E_a}{k_BT}\right) \tag{16}$$

where the static barrier contribution is removed from the observed rate constant, it is possible to determine whether or not the reaction takes place in the Smoluchowski limit or not. Combining Equation (16) with the high-friction Kramers result (Equation 10), setting $F = \frac{\omega_B}{\beta}$, one obtains the reduced rate constant in the Smoluchowski limit of Kramers' theory:

$$k_{red} = \frac{\omega_A\omega_B}{2\pi\beta}. \tag{17}$$

However, it is often the case that reactions are not truly in this limit, and to account for some relaxation from that limit, it has become common to modify the reduced rate constant to [126]:

$$k_{red} = \frac{\omega_A\omega_B}{2\pi\beta^\alpha} \tag{18}$$

where $\alpha$ is determined by a fit and deviations from $\alpha = 1$ indicate the process does not occur in the Smoluchowski limit. A plot of $\ln(k_{red})$ versus $\ln(\eta)$ can be used to deduce $\alpha$ since it will be the slope of the resulting line.

Despite its conceptual simplicity, there is a serious dilemma in adopting the Kramers result and using it to compare with the experiment. Although the microscopic friction is well defined physically in the Langevin equation, it is an altogether different and a more

challenging matter to link this variable to macroscopic bulk solvent properties. By far, the most common is to make the hydrodynamic Stokes–Einstein approximation that the solvent friction is directly proportional to the bulk shear viscosity. The problem with this assumption is that many dynamical quantities are known to become decoupled from solvent viscosity under various conditions, for example, once the solvent molecule becomes larger than the solute itself [127]. Evidence for the departure from Stokes–Einstein can be seen in many examples of orientational diffusion as measured by transient absorption anisotropy or time-resolved fluorescence anisotropy. Recently, we have shown that spectral diffusion of a transition metal carbonyl complex [$Re_2(CO)_{10}$] also becomes dramatically decoupled from solvent viscosity in a glass-forming liquid (1,2-hexanediol) over a very wide viscosity range, only to become hypersensitive to viscosity near the glass transition temperature [99]. Hence, the use of the Kramers result will necessarily rely heavily on the appropriateness of the choice of friction model [126,128]. Indeed, there are elegant extensions to the theory where the simple Markovian model of friction used by Kramers is replaced by a kernel – due to Grote and Hynes – where solvent shell memory effects and dynamics specifically relevant to the reactive crossing can be included [129,130].

Regardless of the specific model of dynamic friction, it is essential to highlight that the Kramers theory result is nearly linear in its dependence on friction, but retains the usual exponential energy dependence of an activated process. Thus, it is always a concern that unexpected, non-dynamical changes to the reaction potential surface may dominate the dynamical contribution due to the solvent friction. From an energetic perspective, any changes in the TS solvation shell structure or its conformational freedom would lead to non-dynamical changes in the rate constant. Notwithstanding the many challenges in directly testing Kramers theory, even using seemingly idealised model reactions, the theory pervades interpretations of many condensed phase chemical phenomena, especially in biophysics [131]. In this section, we describe the first direct test of the dynamical nature of Kramers' theory of activated barrier crossings on a well-defined, unimolecular, ground electronic state reaction using the powerful methodology of ultrafast 2D-IR chemical exchange spectroscopy.

### 3.3.2. *A model isomerisation reaction in $CO_2(CO)_8$*

Dicobalt octacarbonyl [$CO_2(CO)_8$, DCO], which catalyses hydroformylation [132] and Pauson–Khand [133] reactions, is a flexible molecule that can adopt three distinct isomers at room temperature (Figure 7) [134]. Since the barriers to interconversion among the isomers were predicted to be $<5$ kcal/mol, DCO held promise as being compatible with 2D-IR exchange spectroscopy [135,136]. One central challenge, that is also an attractive feature, is the presence of three stable species, which contrasts with other reports of 2D-IR exchange studies. A first step was to show that it is possible to isolate the exchange signal despite the multilevel vibrational structure of all three isomers [5].

The linear FT-IR spectrum recorded at room temperature in *n*-hexane can be fit to seven bands, three arising from bridged isomer I, and two each from the non-bridged isomers II and III. The assignments were determined from low-temperature IR spectra and were confirmed by our 2D-IR results [134].

Absorptive 2D-IR spectra of DCO at $t_2 = 100$ fs and $t_2 = 30$ ps are shown in Figure 8. Negative peaks (blue) result from fundamental transitions (i.e. ground-state bleach and stimulated emission), while the positive peaks (red) are due to excited vibrational

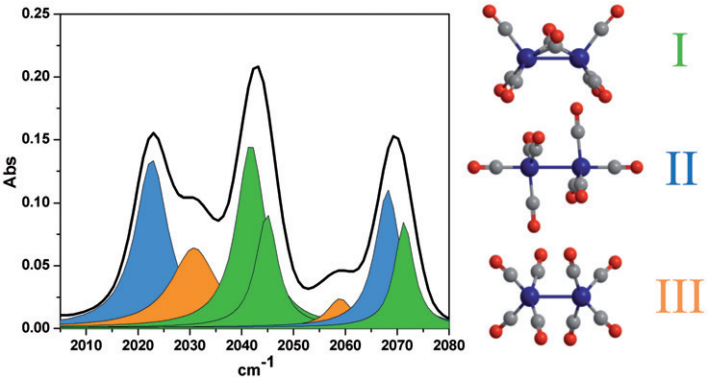


Figure 7. (Colour online) FT-IR spectrum of $CO_2(CO)_8$ with Lorentzian fits assigned to the three isomers (I, II and III) present at room temperature. Adapted with permission from ref. [5]. Copyright 2009 American Chemical Society.

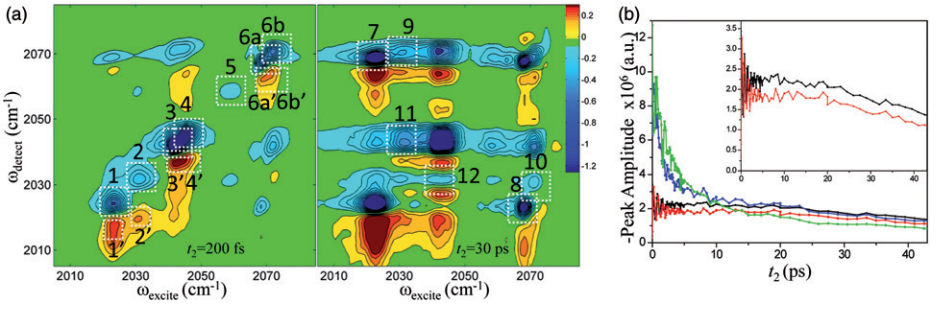


Figure 8. (Colour online) (a) Absorptive 2D-IR spectra of $CO_2(CO)_8$ at $t_2 = 200$ fs and 30 ps and (b) waiting-time-dependent slices for peaks (top to bottom) 6 (green), 1 (blue), 8 (black), and 7 (red); the inset shows only 7 (top) and 8 (bottom). Adapted with permission from ref. [17]. Copyright 2010 American Institute of Physics.

state absorption. The peaks lying along the diagonal correspond to those in the FT-IR spectra; peaks 3, 4 and 6 b are due to isomer I, peaks 1 and 6 a to isomer II and peaks 2 and 5 to isomer III [134]. The induced absorptions are red-shifted along the detection axis with respect to the diagonal peaks because of vibrational anharmonicity. Peaks 3′, 4′, and 6 b′ are assigned to induced excited state absorptions of isomer I, peaks 1' and 6a' are assigned to induced excited state absorptions of isomer II and peak 2′ is assigned to the induced excited state absorptions of isomer III. At early waiting time, cross peaks arise only from coupled modes belonging to the same isomer; the inherent cross peaks present at $t_2 = 200$ fs confirm the assignment of the linear spectrum, highlighting a key capability of 2D-IR spectroscopy.

Although absorptive 2D spectra provide the highest possible spectral resolution, they are more cumbersome to measure since they require both rephasing and non-rephasing data as well as a pump–probe transient absorption spectrum in order to properly phase the two. We have found that in many cases, particularly in the case of the relatively narrow

band metal carbonyl systems, rephasing or non-rephasing spectra alone can provide the dynamical information that we seek, at the expense of an optimal spectral line shape. For example, we have shown that non-rephasing spectra are especially useful for extracting intramolecular vibrational energy transfer (i.e. IVR) [78], and rephasing spectra are suited for observing coherent quantum beating [137]. For the temperature- and solvent-dependent measurements of chemical exchange among DCO's isomers, we have analysed the rephasing spectra.

One of the challenges posed by spectrally congested molecules is that the desired chemical exchange signal is often accompanied by a non-exchanging background due to the coupled nature of the individual chemical species. In DCO, we have found that the strongest and cleanest region of the spectrum to analyse for exchange is at peak 7, which corresponds to exchange between isomers II and I. The exchange contribution to the signal at that location is due to excitation at the lower frequency band of isomer II, followed by detection at the higher frequency band of isomer I. Unfortunately, there is also an overlapping cross peak between the two bands of isomer II, which can have non-trivial dynamics due to IVR, orientational relaxation and population relaxation. In addition to these incoherent dynamics, there is also the coherent oscillation of the background cross peak that arises from a superposition of the two bands of isomer II, which beat at their difference frequency through a well-understood phenomenon inherent to excitonically coupled systems [137,138]. Through a procedure described in detail in the original publications and summarised in Figure 9 [5,17], we use the presence of the coherent oscillations and MD simulations of the orientational correlation functions of each vibrational mode to extract the exchange contribution to the observed waiting-time-dependent cross peak. Temperature-dependent waiting-time slices (Figure 10) showed a clear acceleration in the exchange contribution at higher temperatures. As a simple control, however, we also examined a complex known not to isomerise as a model system to test the influence of temperature on IVR, orientational relaxation and vibrational energy relaxation. Rhodium acetylacetonato dicarbonyl (RDC) is a vibrational dimer system that has become a *de facto* benchmark molecule for both experimental and theoretical 2D-IR spectroscopy [139,140]. RDC has two CO transitions corresponding to the symmetric and antisymmetric stretches, and we analysed the main cross peak between these transitions at two different temperatures of 12°C and 42°C (Figure 11). The two traces are nearly identical even with respect to the strong quantum beat coherence signal, indicating that temperature has a very small effect on IVR, orientational relaxation and vibrational relaxation. The tiny difference we observed was consistent with both the popular theory of IVR and the Debye–Stokes–Einstein (DSE) model for orientational diffusion. Hence, the RDC data provide clear evidence that the very pronounced temperature effects observed in DCO are due to the reactive barrier crossing process.

Having established a method to extract the exchange contribution to the region of the 2D spectrum at peak 7, temperature- and solvent-dependent measurements facilitate estimates of the reaction barrier and the role of solvent friction, respectively. Repeating the waiting-time-dependent 2D-IR scan at several temperatures (Figure 10) yields a series of exchange rate constants, which yield forward and reverse rate constants with the aid of temperature-dependent equilibrium constants obtained from FT-IR spectra. Figure 12 shows Arrhenius and Eyring plots for the II-to-I isomerisation reaction in *n*-hexane solution, indicating the expected trend of faster reaction at increased temperature.

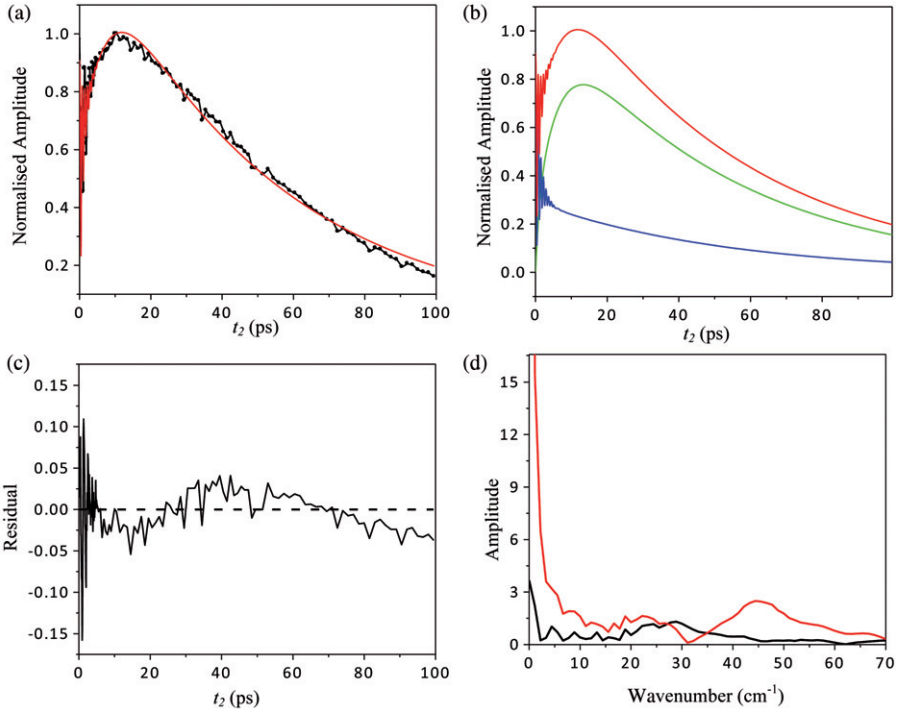


Figure 9. (Colour online) Illustration of method used to remove the background inherent cross peak from the exchange contribution: (a) normalised peak 7 amplitude with the full fit; (b) full fit (red, top), the exchange contribution (green, middle) and the inherent cross peak (blue, bottom); (c) residual of the full fit; (d) amplitudes of FTs of the peak 7 (red, top) and the residual (black, bottom), showing the clear feature at 45 cm$^{-1}$, due to the coherent quantum beating of the two modes of isomer II. Adapted with permission from ref. [17]. Copyright 2010 American Institute of Physics.

A difficulty arises, however, in determining the activation barrier because the of the non-trivial temperature dependence of the solvent's viscosity. For typical reaction barriers (i.e. $>$50 kcal/mol) such an error is not particularly striking, but for low-barrier ultrafast reactions, the viscosity contribution can be of identical magnitude to the barrier itself. Accounting for the viscosity contribution would require some model of its influence on the rate constant, and the first report simply adopted the diffusive Kramers theory result that the rate constant was proportional to the solvent viscosity multiplied by the 1D TST rate constant [5]. Since this reasoning is essentially circular, assuming the validity of Kramers theory, the earlier temperature-dependent study made it evident that the isomerisation of DCO as measured by 2D-IR chemical exchange could be used to test Kramers theory of condensed phase barrier crossings by altering the solvent properties.

One potential pitfall of using Kramers theory without care is the possibility that changing an experimental parameter, such as the solvent, could alter not only the dynamical viscosity, but also the energetics. Since the high-friction Kramers result is essentially linear in the friction but exponential in the energetics, it is critical to ensure that static energetic changes are either avoided or explicitly known. In the case of the 2D-IR

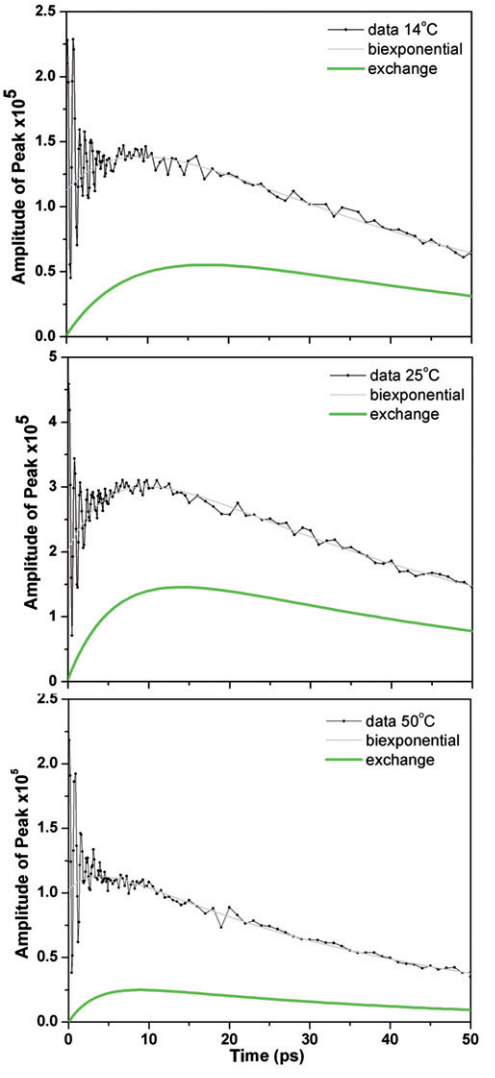


Figure 10. (Colour online) Waiting-time slices from rephasing-only 2D-IR spectra of $CO_2(CO)_8$ in *n*-hexane at 14°C, 25°C and 50°C. The bottom smooth curves in each panel show the extracted exchange contributions. Adapted with permission from ref. [5]. Copyright 2009 American Chemical Society.

chemical exchange studies of DCO, several measurements and calculations were done to assess the degree of solvent-induced modifications of the energetics. FT-IR spectra of the linear alkane series (*n*-hexane to *n*-dodecane) showed negligible changes, indicating that the equilibrium among the three isomers was not affected by the different solvents. Density functional theory calculations of the energies of isomers I and II as well as the TS structures showed no appreciable differences between hexane and decane, modelled using the polarisable continuum solvation method. Possible entropic and hence also non-dynamical effects were also investigated using explicit solvent MD simulations of the

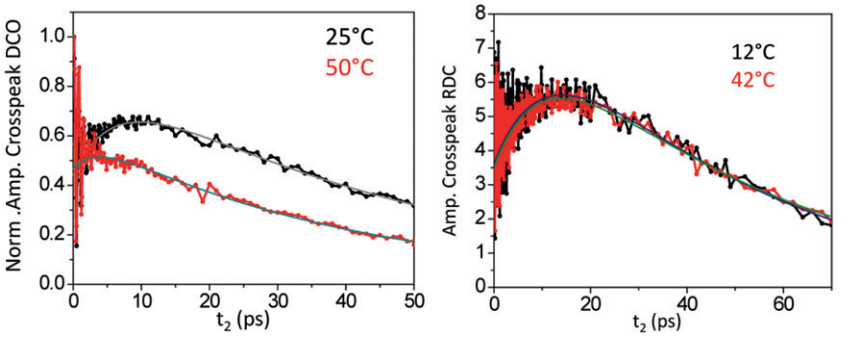


Figure 11. (Colour online) Waiting-time slices from rephasing-only 2D-IR spectra of $CO_2(CO)_8$ at 25°C and 50°C (left) and rhodium dicarbonyl at 12°C and 42°C (right). Adapted with permission from ref. [17]. Copyright 2010 American Institute of Physics.

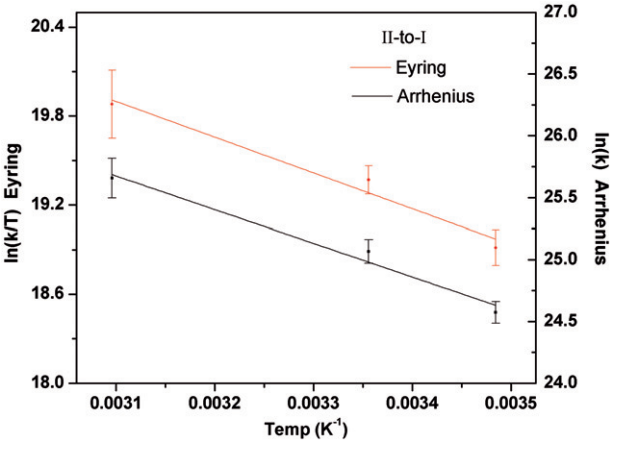


Figure 12. (Colour online) Eyring (top) and Arrhenius (bottom) analyses of the temperature-dependent rate constants for $CO_2(CO)_8$ in *n*-hexane. Adapted with permission from ref. [5]. Copyright 2009 American Chemical Society.

isomers and the TS structures, where the solvation structures were compared using radial distribution functions of the distances from the carbonyl oxygen to all the solvent atoms. Indeed, there were no appreciable differences among the solvents, indicating that even the solvation structures were conserved across the linear alkane series. Since radial distribution functions are related to free energy [103], these simulations provide strong evidence that the reaction energetics are invariant to the alkane chain length.

Having investigated the possible confounding non-dynamical energetic differences, it is reasonable to conclude that the changes to the observed rate constants are attributable to the dynamics of the solvent acting to impede the barrier crossing. Figure 13 shows the measured cross-peak amplitudes for the five solvents hexane, heptane, octane, decane and dodecane. Using the method briefly described above and detailed in [17] to extract the exchange component, the results are summarised in Figure 14, showing a pronounced

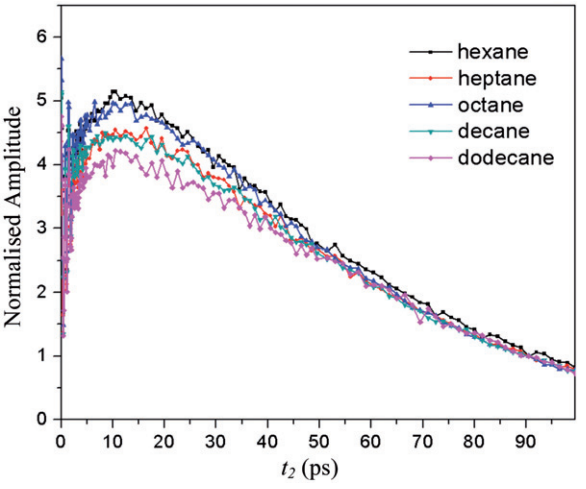


Figure 13. (Colour online) Waiting-time slices from rephasing-only 2D-IR spectra of $CO_2(CO)_8$ in a series of linear alkanes increasing in length from top to bottom. Adapted with permission from ref. [17]. Copyright 2010 American Institute of Physics.

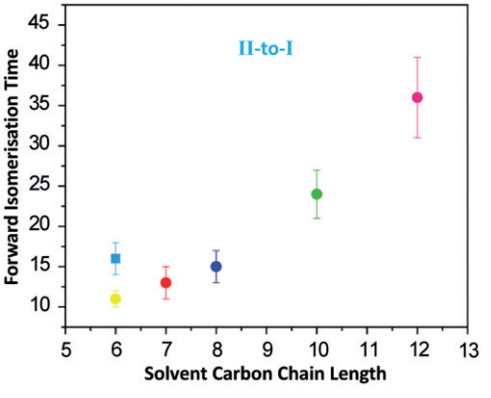


Figure 14. (Colour online) Solvent chain length dependence of the II-to-I rate constant (expressed as a time constant). Circles denote linear alkanes and the squares cyclohexane, which clearly deviates from the linear alkane trend. Adapted with permission from ref. [17]. Copyright 2010 American Institute of Physics.

solvent dependence of the rate constants. Over the range of viscosities, 0.3 cP for hexane to 1.3 cP for dodecane, the reaction rate constants differ by a factor of three. The logarithm of the reduced rate constant data is plotted versus the logarithm of viscosity and orientational time in Figure 15. Since all the slopes give values for $\alpha$ that are less than one (as introduced in Equation (18)), both reactions (i.e. forward and reverse) are slightly below the Smoluchowski limit. Hence, to analyse the data completely, it is necessary to fit to the full Kramers result.

The final potential pitfall of comparing experimental data with Kramers' theory is the choice of a macroscopic model for the microscopic friction. Although it is quite common

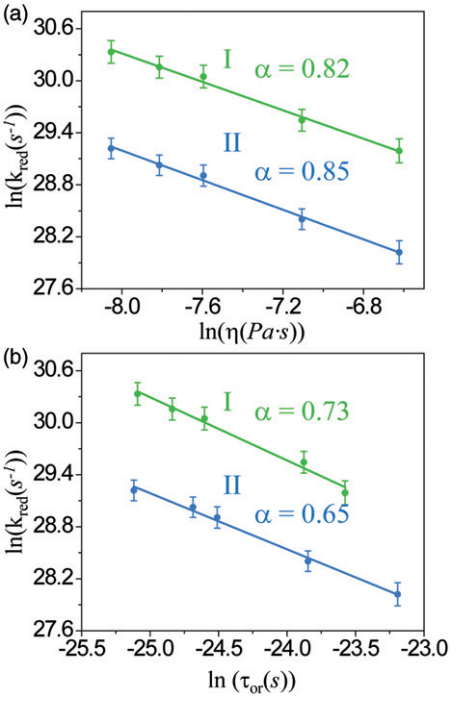


Figure 15. (Colour online) Log–log plots of the reduced rate constants versus viscosity (a) and orientational relaxation time (b) for the linear alkanes. Green (top) refers to the I-to-II reaction and blue (bottom) to the II-to-I reaction. In all cases, $\alpha < 1$, indicating that the reactions are not strictly in the Smoluchowski limit. Adapted with permission from ref. [17]. Copyright 2010 American Institute of Physics.

to employ the Stokes–Einstein result, essentially setting the friction proportional to the bulk shear viscosity, previous work on stilbene isomerisation showed that such an approach can be problematic, especially for large solvents where there is an expected decoupling from viscosity [126,128,141,142]. An alternative method, due to the work of Hubbard [143] in modelling orientational diffusion in the context of NMR spectroscopy, replaced the viscosity with the empirically determined orientational relaxation time $\tau_{or}$. Since orientational relaxation is expected to decouple from viscosity, the idea was that measuring $\tau_{or}$ would include the 'right' solvent dynamical contribution to diffusive reactive motion. Because the orientational relaxation is nearly impossible to measure in a multimode vibrational system with a spectral overlap and chemical exchange, we modelled the orientational relaxation using MD simulations of molecules that were not permitted to isomerise. For the linear alkanes, we found a very simple DSE dependence of the two isomers in the linear alkane series, but for cyclohexane, we found a significant deviation. In order to treat all the measured data together, including cyclohexane, we chose to analyse the Kramers model using the Hubbard model for the friction, where

$$\beta = \frac{6k_B T}{I_{rxn}} p\tau_{or} \tag{19}$$

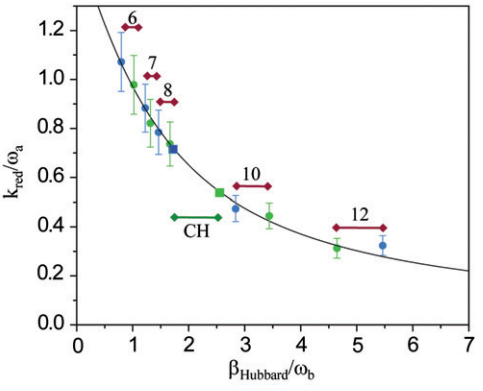


Figure 16. A master curve accounts for the dynamical influence of all the solvents. Using this curve as a constraint and a single measurement of exchange in cyclohexane, which is known to modify the reaction potential surface, it is possible to deduce the forward and reverse barriers assuming that Kramers' theory holds (and that the simulation faithfully yields the orientation time). Adapted with permission from ref. [17]. Copyright 2010 American Institute of Physics.

where $I_{rxn}$ is the moment of inertia of the motion along the reaction coordinate and $p$ a scaling factor that accounts for the imperfect correspondence between the overall molecular reorientation and the reorientation corresponding to the reaction [128].

By recasting the Kramers result slightly, it is possible to deduce a relationship between $k_{red}/\omega_A$ and $\beta/\omega_B$ which decouples the static and dynamic contributions to the rate constant. Such an analysis results in a kind of 'master curve' for the reaction, where the rate constants for both the forward and reverse reactions collapse onto a single curve (Figure 16). Using this curve, it is possible to determine the reaction barrier in a solvent that *does* modify the static energetics, provided one knows the observed rate constants and the appropriate solvent dynamical parameter, in this case $\tau_{or}$ obtained from simulation. The appeal of such an approach is that though the cyclic alkane does alter the equilibrium between isomers I and II, as well as the barriers, it is nevertheless possible to determine the forward and reverse barriers by performing a *single* kinetics measurement.

### 3.3.3. *Current status and future prospects*

There have now been several reports of ultrafast chemical exchange using 2D-IR to study low-barrier chemical reactions. Clearly, the restraints imposed by the short, finite lifetimes of vibrational excited states limit the applicability of the technique to a temporal window roughly <100 ps and hence to barriers roughly <10 kcal/mol. Despite these limitations, many of the most important reactions in biology are within this range, since the chief role of an enzyme is to lower reaction barriers to the extent that the kinetics of many enzymes become limited by substrate diffusion to the active site or by product release after catalysis [144]. A key frontier will be to use ultrafast chemical exchange to probe catalytic active sites, perhaps using inhibitors and TS analogues [145–147]. The goal will be to assess the role played by dynamics in mediating both barrier crossings – from the Kramers perspective of dynamical recrossings – as well as from the energetics perspective of stochastic modulations of the TS barrier [148].

## 4. Non-equilibrium reaction dynamics: photochemistry and photophysics

Since the advent of pulsed lasers and their application to chemical processes, it has been possible to trigger reactions using a pump light pulse and monitor the transformation using a probe. As a continuation of this long tradition, the extension of 2D-IR spectroscopy to the study of transient, non-equilibrium phenomena offers the spectroscopic advantages of 2D spectroscopy while still providing access to photochemical and photophysical events. First demonstrated by Bredenbeck *et al.* [23,149] using a remarkable photoswitchable peptide, several groups have implemented various versions of transient 2D spectroscopy, focusing on systems that include ligand dissociation [150], electronic excitation [96], bond breaking [25,27,51], isomerisation [151], geminate rebinding [31], protein folding [33,152] and charge transfer [32]. These experiments are quite demanding, putting Draconian requirements on available signal-to-noise ratios and introducing 2D bleach signals. Given these difficulties, progress in transient 2D spectroscopy has been slower than in other applications of 2D spectroscopy. With invigorated interest in photosynthesis and artificial photovoltaics and photocatalysis, however, these methods are certain to receive increased attention in the coming years. This section briefly introduces the experimental approaches and some applications in photochemistry and photophysics.

### 4.1. *Brief survey of transient 2D-IR*

Simplistically, transient 2D spectroscopy is an ordinary 2D measurement with an additional pulse that initiates a chemical or physical change. In practice, there have been two versions of transient 2D spectroscopy which we denote 'pump–probe' and 'triggered-exchange'. The pump–probe method treats the 2D-IR spectral measurement as a probe of the non-equilibrium system prepared by the 'actinic' pump pulse [26]. The second pulse sequence involves an actinic pulse between the IR excitation and the IR detection, causing an abrupt change in the electronic state of the vibrationally labelled molecules [26,95]. The detected signal corresponds to molecules that have been excited both by the IR frequency corresponding to the IR excitation axis, and by the actinic pulse. Ideally, triggered-exchange allows a mapping of ground electronic vibrational states to the excited electronic manifold. The potential value of this information is evident since it is generally a straightforward matter to compute ground-state vibrational modes, whereas there is little current hope of equal success on an electronic excited state. The ability to essentially project the excited-state vibrations onto the basis of the ground-state modes would 'solve' the excited-state vibrational problem experimentally – a tantalising goal, but one that has yet to be achieved experimentally. For slower transient processes, where the vibrational Hamiltonian changes gradually, the vibrational modes may be thought of as following the reaction coordinate, in analogy to adiabatic passage [153].

Whether the IR pulses are implemented in the background-free, hole-burning or pump–probe geometry, the basic experimental implementations are nearly identical. That is, to date, there have been no fully coherent implementations of combined electronic/vibrational fifth-order spectroscopy, and all measurements can be thought of as differences between ordinary 2D spectra. The inevitable drawback of actinic pump modulated 2D-IR spectra is the presence of very strong 2D bleach signals; these bleaches could in principle be eliminated by a fully non-collinear beam geometry. We note that the third-order version has recently been achieved using an IR-probed UV transient grating [154].

The number of systems studied with transient 2D-IR is somewhat limited. Hamm and other researchers have investigated protein dynamics using a photoswitchable peptide, based on an azobenzene switch and isotope-labelled peptides [18,21–24,149,155]. They have also studied the structural evolution within a beta turn by photocleaving a disulphide bond [27]. They have developed triggered exchange using an organometallic complex that undergoes metal-to-ligand charge transfer promptly following electronic excitation [95]. Using triggered exchange, they have been able to map the carbon monoxide docking sites within myoglobin to the heterogeneous protein conformational substates [156]. Cervetto *et al*. [151] studied the isomerisation of a thiopeptide revealing hidden vibrational features in the photoproduct. Xiong *et al*. [96] investigated a similar organometallic complex in its role as a photosensitiser on $TiO_2$ nanoparticle surfaces, showing that there are at least two binding modes at the semiconductor interface. Tokmakoff and other researchers have used temperature-jump pulses to transiently heat water and partially unfold proteins, which are then tracked by 2D-IR in order to map structural changes to the amide-I band of the peptide backbone [33,152,157]. Hunt and other authors have studied iron hydrogenase model compounds, which are small metal carbonyl complexes, producing photoproducts that might serve as candidates for $H_2$ generation [29,51,79]. In the following section, we summarise our investigations of photocleavage and transient cooling of hot photoproducts, in-cage geminate rebinding and ultrafast charge transfer from the perspective of the first solvation shell.

### 4.2. *Photodissociation of $Mn_2(CO)_{10}$: watching photoproducts cool*

Photodissociation, a mainstay of ultrafast chemical reaction dynamics, involves optical excitation via an allowed transition that ultimately leads to bond cleavage, where the bond dissociation energy is generally less than the incident energy per photon. Hence, prompt photodissociation is accompanied by rapid local heating, first of the photoproduct and then of the local solvent environment. For small molecules with low heat capacities, it is not uncommon for photochemical reactions to cause hundreds of degrees of temperature rise, although it is worth noting that the system is at least initially not at equilibrium and the concept of temperature must be taken somewhat loosely. Nevertheless, assuming a rapid, sub-picosecond photocleavage event, some degree of thermalisation can take place.

One question that can be addressed using transient IR and transient 2D-IR spectroscopy is: 'how long does it take photoproducts to cool?' One way to sense photoproduct cooling is to measure the transient IR absorption line width as a function of time following the optical trigger pulse [158]. The temperature jump is initially confined to the photoproduct solute and manifests itself as a spectral broadening due to anharmonic coupling to the low-frequency modes of the nascent species. By monitoring the time dependence of the width, it should be possible to estimate the cooling and hence to establish a transient molecular thermometer [159–161]. This approach can become complicated or impractical when there are multiple overlapping bands, and it is also a challenge to make a direct link between spectral width and temperature.

Another way to determine transient 'temperature' would be to measure transient orientational relaxation, which at least for many systems obeys a rather simple temperature dependence due to the DSE model that relates the orientational relaxation

time $\tau_{or}$ to the temperature as

$$\tau_{or} = \frac{C\eta v_m}{k_B T} \tag{20}$$

where $C$ is an empirical constant that depends on the tumbling molecule's shape, $\eta$ is the solvent's viscosity and $v_m$ is the molecular volume of the solute. For an equilibrium system, orientational relaxation will have two sources of temperature dependence, that due to the temperature itself and the indirect effect through the temperature-dependent viscosity. For a transient non-equilibrium system, however, it is possible that the thermal transfer from the solute to the solvent is slow enough, and the heat capacity of the local solvent is high enough that the immediate solvation shell remains at a constant temperature. As we show below, this scenario describes well the case of transition metal carbonyl photochemistry.

To use orientational relaxation to probe temperature is distinct from traditional transient absorption anisotropy, where two pump–probe spectra, recorded with parallel and perpendicular relative polarisations are used to compute a time-dependent anisotropy. Ordinary anisotropy decays will only report on the loss of orientational correlation between the initially excited parent species and the evolving daughter product. Instead, what is needed is a *transient*, transient anisotropy measurement where the evolving time scales for orientational relaxation are determined as a function of a presumably longer time following the photochemical trigger. Since a 2D-IR spectrum contains orientational relaxation, it is possible to extract that information from the transient 2D-IR spectra, though a reliable assignment requires some knowledge of the parent and daughter species' reorientation times. In this section, we describe how to record transient temperature using the time-evolving orientational relaxation contained in transient 2D-IR spectra of $Mn_2(CO)_{10}$ in a non-polar solvent.

Dimanganese decacarbonyl (DMDC, Figure 17) undergoes two different photodissociation pathways in solution depending on the optical excitation wavelength [162]. Shorter wavelength (<300 nm) induces single CO loss, producing $Mn_2(CO)_9$ [163,164], whereas longer wavelength (>300 nm) favours primarily Mn–Mn cleavage, resulting in two $Mn(CO)_5$ monomers [165]. The parent DMDC, which has been studied in extensive detail using 2D-IR spectroscopy, is characterised by its three main CO stretching bands corresponding to the four IR allowed transitions (two of which are degenerate) [78,137,166–168]. Following photodissociation at 400 nm, the pentacarbonyl monomers absorb in a relatively broad band centred around 1980 $cm^{-1}$, which unfortunately sits atop the low-frequency band of the parent complex [158]. Nevertheless, the transient absorption and the transient 2D-IR spectrum of the photoproducts can be followed as a function time between the actinic pump and the 1D or 2D-IR probe. The 1D measurements had been reported previously by Steinhurst *et al.* [158] and our measurements were consistent with theirs. A key observation in transient IR absorption measurements is that of a transient photoproduct absorption spectral width, which is broad immediately following photodissociation and narrows as the photoproducts cool. The broad line shape is due to anharmonic coupling to low-frequency modes that gain population by the deposition of heat into the nascent photoproduct. In the case of $Mn_2(CO)_{10}$, the excess energy distributed between the two fragments upon 400 nm dissociation is 12,000 $cm^{-1}$. Given the heat capacity of the $Mn(CO)_5$ monomers and assuming equal partitioning of the excess thermal energy (i.e. 6000 $cm^{-1}$ per fragment), the predicted transient temperature

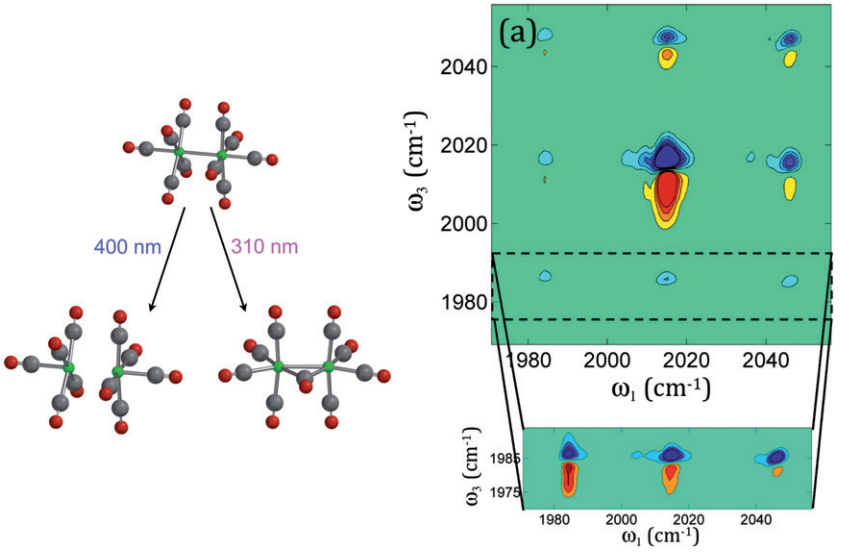


Figure 17. (Colour online) (left) Structure of $Mn_2(CO)_{10}$ (DMDC) and its excitation wavelength dependent photoproducts. (right) Absorptive 2D-IR spectrum of DMDC in *n*-hexane at a waiting time of 5 ps, with a recontoured zoom of the detection window near 1985 $cm^{-1}$. Adapted with permission from ref. [62]. Copyright 2010 Optical Society of America.

rise is ~300 K. This low temperature is insufficient to excite high-frequency vibrations, though earlier transient IR work on $W(CO)_6$ dissociation in the near-UV clearly produced CO vibrational excitation in the $W(CO)_5$ photoproduct [169]. Any heating that excites high-frequency modes would lead to new cross peaks in the transient 2D spectrum, in keeping with the fifth-order nature of the experiment. So far, these excitation-induced features have not yet been reported.

The series of transient 2D-IR spectra (Figure 18) recorded at various times following the photodissociation permit the determination of dynamics by scanning the internal delay within the 2D-IR probe. That is, with the 2D-IR spectrum as an observable, the full data set becomes 2D in two different times, that following the phototrigger ($\tau$) and the 2D-IR waiting time ($t_2$). Although there are, in principle, more detailed analyses of the transient spectra, given the limitations of signal-to-noise ratios and the spectral overlap with the parent bleach, the set of transient spectra were simply integrated. Hence, at each value of phototrigger delay and 2D-IR waiting time, we integrate the amplitude of induced 2D rephasing signal (red regions of the 2D spectra). This analysis shows that the 2D spectra decay according to a biexponential relaxation, with a $\tau$-independent rapid component of 1–2 ps and a slower component that does depend on $\tau$. The UV–IR delay dependence of the slower component is shown in Figure 19. The decay in the time constant follows an exponential with a time constant of $70 \pm 16$ ps, indicating that the rate of 2D signal decay becomes slower with increased UV–2D-IR delay. That is, as the photoproducts cool, the slow component of the 2D-IR signal decay becomes slower.

The 2D-IR decays ranged from 2.5 ps (at $\tau = 40$ ps) to 12 ps ($\tau = 300$ ps), suggesting an orientational relaxation origin, since the vibrational lifetime is much longer, as is

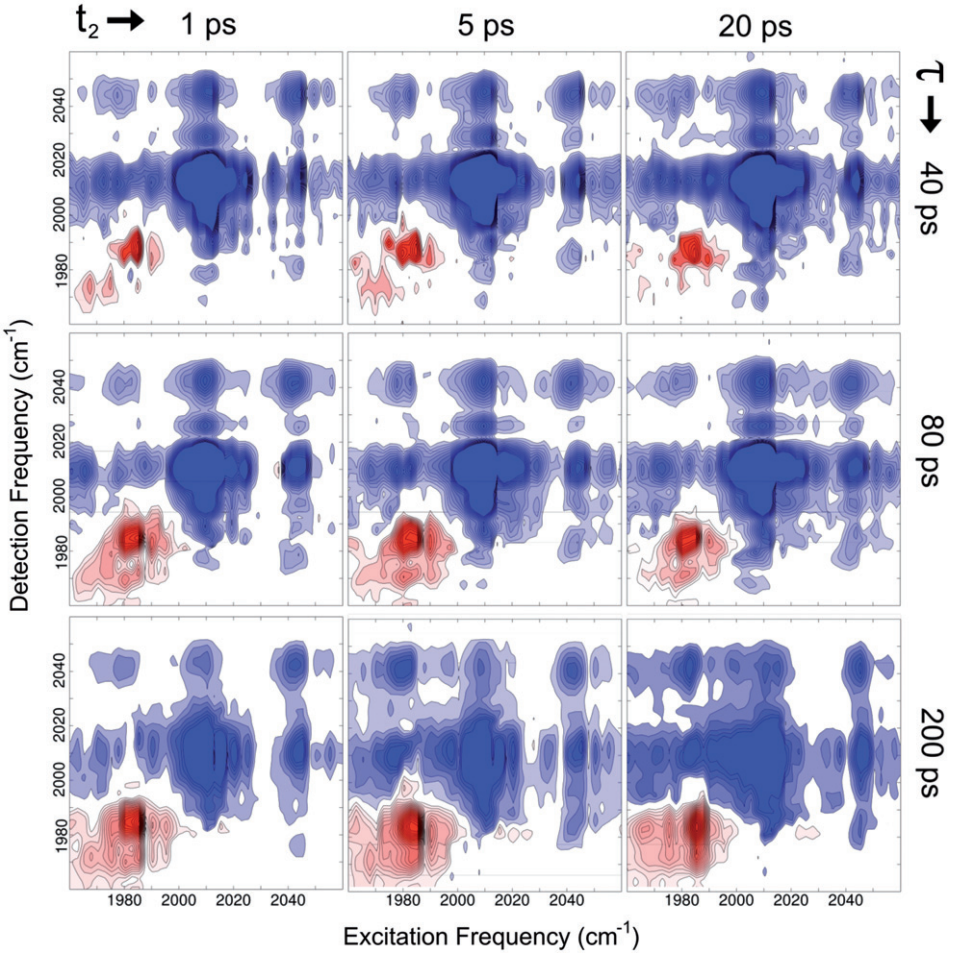


Figure 18. (Colour online) Representative transient 2D-IR spectra of $Mn_2(CO)_{10}$ in cyclohexane shown at three UV–IR delays (40, 80 and 200 ps) and at three 2D-IR waiting times (1, 5 and 20 ps). Red (centered near 1980 $cm^{-1}$) contours are induced 2D signal from $Mn(CO)_5$ monomers and remaining contours correspond to the bleach of the parent molecule. Adapted with permission from ref. [25]. Copyright 2009 American Chemical Society.

evidenced by the offset in the 2D-IR peak volumes seen at the latest waiting-time delay. Using transient absorption anisotropy of the DMDC parent in cyclohexane, we determined the orientational relaxation time to be $15.8 \pm 3.5$ ps, consistent with the molecule's size and the known viscosity of cyclohexane. Using equilibrium MD simulations of the parent and the monomer photoproduct, we computed orientational correlation times of 18.2 and 11.7 ps, respectively. The faster orientational relaxation of the monomer is consistent with its smaller size. The close agreement between experiment and simulation for the parent indicated that the relaxed monomer's orientational relaxation could be well estimated from the simulation to be roughly 12 ps, which is the same value found for the longest time 2D-IR signal decay in the transient experiment.

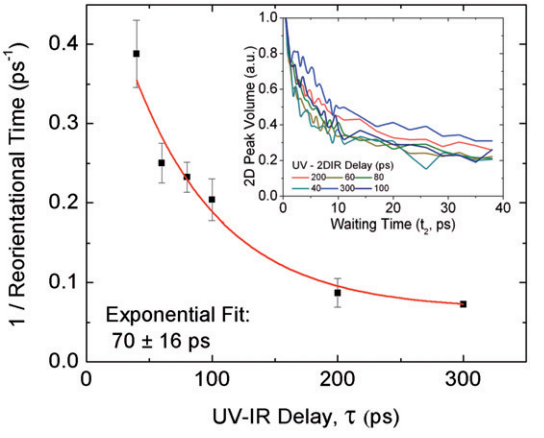


Figure 19. (Colour online) (inset) Decays of induced transient 2D-IR amplitude at six different UV–IR delays (40, 60, 80, 100, 200 and 300 ps). The main plot shows the UV–IR delay time dependence of the slow relaxation components (in ps$^{-1}$) of the fits to the decays in the inset. A single exponential decay with a time constant of $70 \pm 16$ ps captures the slow down in 2D-IR relaxation as the initially hot photoproducts cool. The final point at 300 ps matches the simulated equilibrium monomer reorientational time of 12 ps. Adapted with permission from ref. [25]. Copyright 2009 American Chemical Society.

By roughly 300 ps, the monomer photoproducts are essentially equilibrated, and the initial 2.5 ps 2D-IR decay evidently corresponds to the initially hot photoproducts.

One of the challenges in interpreting these experiments is the inherently non-equilibrium nature of the photodissociation. There are certainly well-known theories for the temperature dependencies of vibrational relaxation, orientational diffusion and IVR, but these are generally formulated from the perspective that the solute and the environment are in equilibrium except for the relaxing degree of freedom. That is, they share a common temperature. Given how weakly coupled DMDC is to its environment, as evidenced by the very narrow $\sim 3\,\mathrm{cm}^{-1}$ IR transitions and the long $\sim 100$ ps vibrational lifetime, we considered the possibility that the solvent molecules remained essentially at room temperature throughout the cooling process. To simulate this scenario, we used non-equilibrium MD simulations to monitor the transient temperatures of the photoproducts and the solvent shell. Indeed, although there was quite a significant time-scale disparity, the solvent molecules were found to remain at room temperature despite the $\sim 300$ K temperature jump of the photoproduct. Although the disagreement in thermal energy dissipation suggests much work remains in developing force fields that can function under thermally non-equilibrium conditions, this study introduced transient 2D-IR spectroscopy as a method to probe thermal relaxation.

### 4.3. *Geminate rebinding of $[CpMo(CO)_3)]_2$: a reaction in a nanovacuum chamber*

In contrast to the relative ease with which light can break chemical bonds, their controlled and synchronised formation is an open challenge for ultrafast reaction dynamics investigations [170]. One example of a bond-forming event that can be optically triggered

is the rapid geminate rebinding of photodissociated species that remain within a solvent cage. As an extension to the classical experiments of Rabinowitch and Wood [171] and Franck and Rabinowitch [172], we examined an organometallic complex, $[CpMo(CO)_3]_2$ in ethyl acetate solution, which is sufficiently polar to permit population of the otherwise energetically unfavourable *gauche* conformation. Tyler and other researchers have explored the use of the molybdenum dimer as a photocatalyst for degradable polymers and have performed several studies investigating the geminate rebinding of photogenerated radicals [173–180]. Much of that work has focused on the involvement of partial or complete solvent separation of the radial pair prior to recombination. Our aim in studying this dimer species was to use the highly efficient geminate rebinding as a means to observe the in-cage reformation of the *trans* and *gauche* isomers based on our assignment of the dimer absorption spectrum using equilibrium 2D-IR spectroscopy [31]. What we found instead was the rather surprising observation that only the *trans* rebinding product formed on the <50 ps time scale, with no evidence of the formation of the *gauche* dimer despite the fact that the equilibrium ratio of *gauche* to *trans* is roughly 1 : 4. Thus, this result shows how transient IR spectroscopy can be used to track evolving molecular species with essentially indistinguishable visible absorption spectra. In this case, we were able to watch an asymmetric, kinetically controlled bimolecular reaction and found, as we will describe below, the solvent to play virtually no role at all in determining the reaction time scale.

The linear IR spectrum of $[CpMo(CO)_3]_2$ is characterised by three bands in the carbonyl stretching region in polar solvents at 1912, 1958 and 2013 $cm^{-1}$. The two low-frequency bands have contributions from the *trans* and *gauche* conformations, whereas the 2013 $cm^{-1}$ band is only due to the *gauche* conformation. It has been previously observed that in non-polar solvents, where the *trans* conformation is highly favoured, the high-frequency band is not present and the low-frequency bands become narrower [181]. Thus, it was predicted that the two isomers would have overlapping transitions near 1913 and 1958 $cm^{-1}$. This assignment is confirmed by the equilibrium 2D-IR spectrum shown in Figure 20. The spectrum shows cross peaks between all three main diagonal peaks. At zero waiting time, the only possible route to cross peaks is a common ground state between the transitions; therefore, in addition to the high-frequency transition, the *gauche* isomer has transitions that overlap those of the *trans* isomer. Since the two isomers are in thermal equilibrium, in principle, it is a possibility that chemical exchange could lead to the growth of these cross peaks at later waiting times. From NMR experiments, however, it is known that the interconversion occurs on the millisecond time scale [181]. Hence, any cross peaks that arise must belong to the same species. This simple peak assignment is one clear example of the inherent structure-specific spectral information provided by 2D-IR spectroscopy.

Optical excitation at 400 nm induces the homolytic cleavage of the Mo–Mo bond. The products of this ultrafast reaction can be studied by transient 2D and transient DVE spectroscopy, yielding insight into the rebinding kinetics and yield. Figure 20 shows the transient 2D-IR spectrum recorded at a 5 ps delay between the UV and the second IR pulse of the three-pulse IR echo sequence (the IR waiting time was set to zero). This spectrum shows the expected 2D bleach spectrum, coloured in blue, corresponding to the loss of parent dimer molecules, as well as the induced 2D signal, coloured in red, due to the monomer photoproduct. The main induced feature is the strong band at 1995 $cm^{-1}$, corresponding to the 17-$e^-$ radical monomer. Since this species is a tricarbonyl, it would be

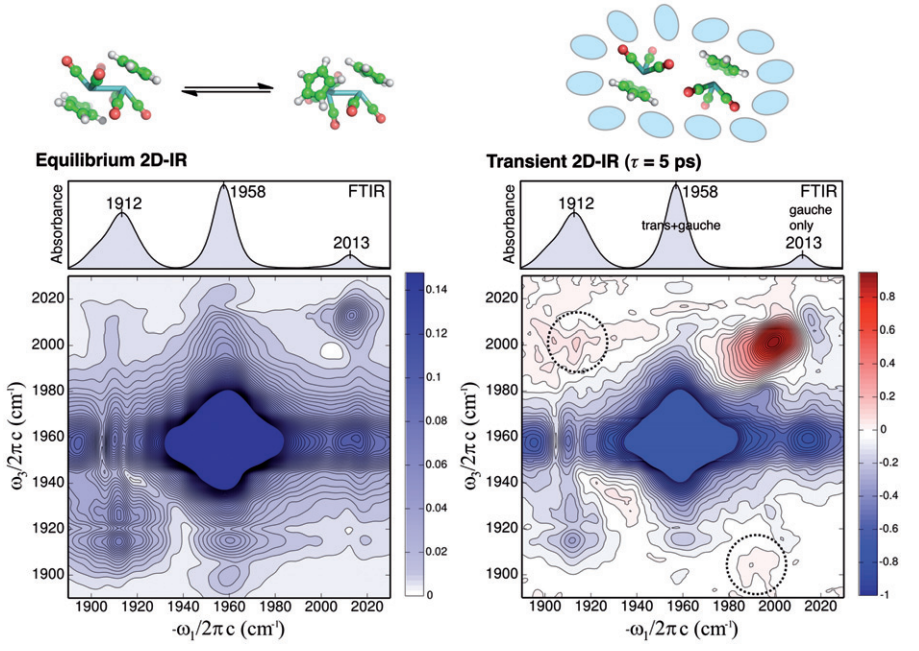


Figure 20. (Colour online) Equilibrium (left) and non-equilibrium (right) structures and 2D-IR spectra for $[CpMo(CO)_3]_2$ in an ethyl acetate solution. The equilibrium FT-IR spectrum is reproduced to aid in comparing the two 2D spectra. The dotted circles in the transient 2D spectrum show the cross peaks between the strong induced diagonal peak and the obscured low-frequency diagonal peak. This transient 2D-IR spectrum is noteworthy as it is recorded as close as possible to the photodissociation event (5 ps). Adapted with permission from ref. [31]. Copyright 2009 American Chemical Society.

expected to have another band at lower frequency, and that has been observed in other transient IR studies [181]. We see evidence for two induced cross peaks between the strong 1995 $cm^{-1}$ band and the lower-frequency band at 1910 $cm^{-1}$. This peak is not seen on the diagonal due primarily to the strong parent dimer bleach, but the cross peaks, which do not suffer an overlapping bleach can clearly be seen in the transient 2D spectrum. Using the transient 2D-IR spectrum, therefore, we are able to assign the nascent photoproduct's vibrational spectrum experimentally.

To measure the rebinding kinetics, it would be ideal to use a series of transient 2D-IR spectra, but limitations in the signal-to-noise ratio and in experimental acquisition time preclude this approach. Instead, given the assignments of the parents and the daughter species, we employed a transient 1D non-linear measurement termed the 'DVE'. [97,98]. Here, the signal is sent directly to the spectrometer without a heterodyne local oscillator, providing a truly background-free spectral measurement, ensuring high signal-to-noise ratios. Because the measurement is non-linear, the excited-state IR absorption also contributes to the homodyned signal, but this interference only adds to the spectral width of the measured signal. Another point of potential complication is the use of a homodyne-detected non-linear optical probe. Naively, one might conclude that such a measurement would be sensitive to the square of the population change of molecules as they rebind,

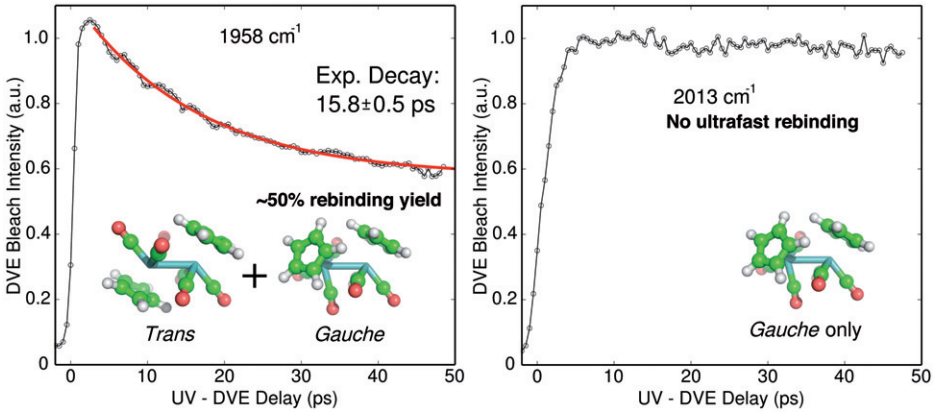


Figure 21. (Colour online) Transient DVE bleach recoveries probed at 1958 $cm^{-1}$ (left) and 2013 $cm^{-1}$ (right). The lack of bleach recovery due to rebinding to the *gauche* isomer indicates that all ultrafast rebinding occurs to the *trans* form. This result is a clear example of how IR spectroscopy can reveal structurally specific, kinetically controlled chemical reaction dynamics. Adapted with permission from ref. [31]. Copyright 2009 American Chemical Society.

leading one to double the observed rebinding rate constant to arrive at the true rebinding rate constant. A careful analysis, however, shows that at sufficiently low bleaches, such as the level of 5% used here, the signal is effectively linear. Hence, to a high degree of confidence (detailed explicitly in ref. [97]), the rebinding rate constant extracted from a transient homodyne DVE measurement is the same as would be found in a conventional transient IR experiment.

Using transient DVE, we monitored the bleach recovery at the two key locations of the parent IR spectrum, at the central 1958 $cm^{-1}$ band corresponding to both *trans* and *gauche* isomers, and at the 2013 $cm^{-1}$ band corresponding to only the *gauche* isomer (Figure 21). The rebinding kinetics are clearly distinct, showing substantial rebinding in the *trans* + *gauche* band, but none at all for the *gauche*-only band. Hence, we conclude that all the ultrafast in-cage rebinding results exclusively in the formation of the *trans* isomer. A relatively simple potential energy surface including the Mo–Mo bond distance and the torsion about that bond supports the experimental observation. At long separations of roughly 2 Å beyond the equilibrium bond length, thermal fluctuations are sufficient to fully randomise the torsional angle distribution. Upon approach, however, the *trans* channel is favoured, with a branching point roughly 1 Å beyond the equilibrium Mo–Mo distance. The agreement with the gas-phase potential energy surface supports a view that this rebinding reaction takes place with little involvement from the solvent, which appears to act simply as an inert nanovacuum chamber keeping the reacting fragments close to each other. Although the solvent appears to be acting as a passive bystander, these results do reveal dynamical insights about an asymmetric reaction that has two thermodynamically viable rebinding products. The observation of exclusive *trans* rebinding is a clear indication that the ultrafast bimolecular reaction is kinetically controlled, and is driven by the shape of the potential surface somewhat distant from the final configuration. The ultimate fate of the reaction is to produce a mixture of *trans* and

*gauche* isomers, but our measurements show that the picosecond primary association necessarily precedes the orders-of-magnitude slower millisecond thermal equilibration.

To test further the idea of an inert solvent cage, we used a non-polar solvent system composed of the branched alkane squalane and *n*-hexane. Hexane–squalane solutions should have a minimal effect on the energetics of the solvent cage, while allowing a tunable viscosity. In the non-polar solvent, there is no detectable *gauche* species, and again, all the rebinding was found to produce the *trans* dimer. By varying the hexane–squalane ratio, we can tune the viscosity from 0.3 cP for pure *n*-hexane to 8 cP for an 80 : 20 squalane : *n*-hexane (v/v) solution [182]. The rebinding time scales in all these solvents were found to be identical (Figure 22), indicating that the reaction rate is truly insensitive to solvent dynamics, but is rather determined by the size of the cavity defined by the monomer species in the solvent cage. Though there was no viscosity dependence to the rebinding rate constant, the yield did in fact correlate with viscosity. In *n*-hexane (0.3 cP), the rebinding yield was found to be 58%, whereas in the 80 : 20 solution (8.0 cP), the yield was 71%. The viscosity dependence of the rebinding yield indicates that the solvent cage is more leaky at lower viscosity, a trend found in earlier transient visible absorption measurements.

Perhaps counterintuitively, the rebinding of $CpMo(CO)_3$ radicals within a solvent cage essentially follows the course expected of isolated molecules in an inert vessel. Since the potential energy surface indicates no transverse barrier along the Mo–Mo bond coordinate, the reaction is largely determined by diffusion in the solvent cavity and by the asymmetry of the potential surface favouring the *trans* isomer. It would be revealing to test this solvent invariance using various substituted Cp rings, as has been studied using transient visible absorption. More broadly, this study provides an insight into the molecular nature of dynamics in confined spaces, where excluded volume effects often dominate both the dynamics and energetics.

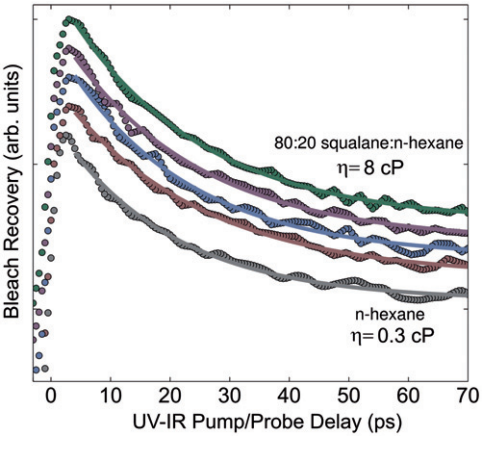


Figure 22. (Colour online) Solvent viscosity dependence of the rebinding kinetics and yield in *n*-hexane and *n*-hexane–squalane mixtures. The curves are offset for clarity, and fits reveal identical rebinding time constants. Rebinding yield, however, was viscosity dependent, increasing with increased viscosity, indicating viscosity-dependent cage escape. Adapted with permission from ref. [179]. Copyright 2011 Oxford University Press.

### 4.4. *Photoinduced charge transfer: the view from the first solvation shell*

In the non-equilibrium reactions described above, a key theme is the apparent lack of solvent involvement in the dynamics that are probed with the transient 2D measurements. In a sense, these findings appear to support the view that the condensed phase environment merely perturbs slightly the isolated molecule picture. Perhaps, such a subordinate role is not surprising given the large amplitudes and high energy scales associated with the reactions. By contrast, in the equilibrium isomerisation case considered in Section 3, we found clear and striking solvent influence on the reactive crossings. Thus, it seems quite natural that the precise role of the solvent will depend on the nature of the solute and the reaction energy landscape.

One class of reactions where we would expect a strong solvent role is in charge transfer [183]. A key ingredient in charge-transfer energetics is the reorganisation of the solvent in response to a charge separation or neutralisation. Ultrafast photoinduced charge-transfer reactions have been studied for decades using transient spectroscopy such as visible absorption, and one of the distinguishing features is the observation of solvent-dependent time scales and quantum efficiencies. Indeed, a solvent polarity dependence is often viewed as sufficient to assign the existence of a charge-transfer state. The standard picture of charge transfer in polar solvents is shown in Figure 23, where, in this case, we start with a molecular species that is effectively zwitterionic due to a large ground-state charge separation solvated by polar solvent molecules. As this solute undergoes a photoinduced charge transfer to a neutral species, the polar molecules will reorient and compress or expand (i.e. electrostrict) in response to the new electrostatic environment. This charge transfer and associated solvation will affect the optical properties of the solute (either absorption of emission, or both), allowing direct spectroscopic access to both the charge-transfer kinetics and the solvation dynamics. It remains a challenge, however, to extract the two contributions separately from a transient electronic absorption spectrum, since the two processes are often so tightly coupled.

Despite decades of progress in studying condensed-phase charge transfer and solvation dynamics using the spectroscopy of the solute, there have been almost no attempts to study the molecules in the first solvation shell – those closest to the action [184]. Of course, the reason is that in typical dilute solutions of reacting solutes, the fraction of molecules in the

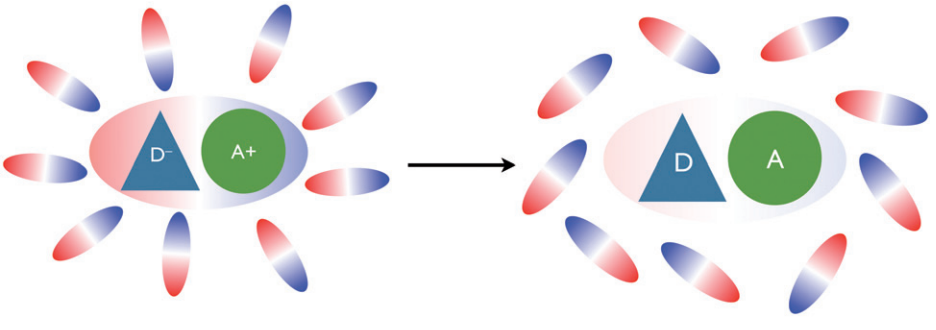


Figure 23. (Colour online) Cartoon depiction of polar solvation of a zwitterionic (i.e. charge-separated ground state) dye molecule. Photoinduced charge transfer transiently extinguishes the constraining electrostatic trap, allowing the solvent shell to relax.

first solvation shell is vanishingly small. We set out to address this problem by devising a ternary system where a visible absorbing charge-transfer dye is preferentially solvated by a strong IR active vibrational probe, all embedded within a background solvent [32]. The charge-transfer system we describe here is the solvatochromic Reichardt's dye (betaine-30, Figure 24) [185], which undergoes an instantaneous charge-transfer reaction to neutralise a large 17 Debye ground-state dipole moment [186–205]. The vibrational probe was the NaSCN contact pair, which forms in the background solvent ethyl acetate [206]. Because the NaSCN contact pairs are more polar than the ethyl acetate, they preferentially solvate the betaine-30 solute. Below, we describe how we were able to use transient changes in the vibrational spectrum of the NaSCN probes in the first solvation shell to sense the ultrafast back electron transfer (bET) following visible excitation of betaine-30.

Betaine-30 is a sensitive solvatochromic molecule that provides the basis for the $E_T30$ scale of solvent polarity [185]. In the ground electronic state, betaine-30 has a very large ~17 Debye dipole moment, so large, in fact, that the molecules can be oriented in solution using a static electric field [205,207]. Upon electronic excitation, the Franck–Condon excited state is a charge-transfer state, essentially neutralising the dipole moment instantly. Early transient absorption spectroscopy studies by Barbara and others showed that solvent-dependent bET occurs on the few picosecond time scale [202–204,208]. Using aligned molecules, Beard *et al.* [205,207] used the terahertz emission of the accelerating electrons undergoing bET to deduce the same ~2 ps bET time scale. Hence, in a range of solvents, the charge 'reseparation' in betaine-30 takes place on a time scale that is somewhat slower than the fastest phase of solvation dynamics, but slower than the characteristic orientational diffusion times of any but the fastest of solvent species (i.e. water). In the present ternary system, the expectation would be the following: the initial charge neutralisation instantaneously reduces betaine-30's dipole moment, relieving the trapping potential on the nearby dipolar NaSCN solvent shell probes, but before they have

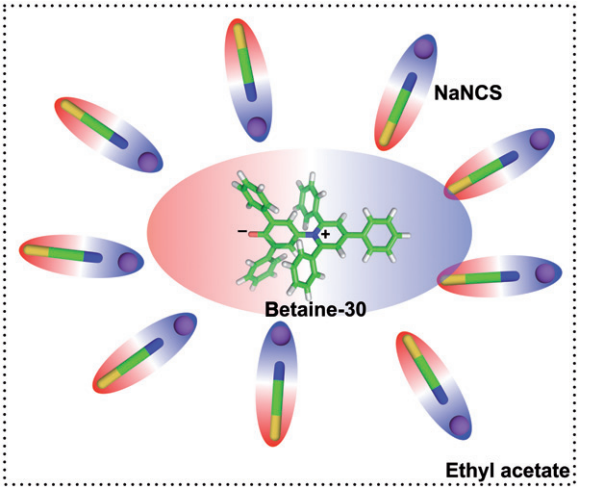


Figure 24. (Colour online) Ternary system used in the dynamic VSE experiments. Betaine-30 (Reichardt's dye) is preferentially solvated by sodium thiocyanate ($Na^+NCS^-$) contact pairs in the less polar ethyl acetate solvent.

time to diffuse orientationally or translationally, rapid bET reestablishes the charge-separated electronic structure, which again traps the solvent shell. What, then, enables a vibrational probe of the bET reaction?

A molecule or a functional group placed into a static electric field can experience a vibrational frequency shift due the vibrational Stark effect (VSE) [209,210]. There are two basic physical origins of the VSE: a geometrical (i.e. structural) distortion due to the electric field and a contribution due to the anharmonicity of the vibrational potential. Although the latter, anharmonic term is the most intuitive, where the nuclear Hamiltonian gains terms proportional to powers of the displacement times the static field through a dipole interaction, theoretical studies have shown that the dominant term is actually that due to the geometrical distortion of the molecule [209]. A key parameter that is needed in order to deduce a local field from an observed frequency shift is the Stark tuning rate, which is the frequency shift (typically in $cm^{-1}$) per unit of electric field (typically in MV/cm). A detailed study by Brewer and Franzen [209] showed that the Stark tuning rates of promising vibrational probes (CO, $CN^-$, alkanenitriles, etc.) are underestimated if the geometries are not first optimised in the applied field. The VSE has been invoked to explain site-specific vibrational frequency shifts of probes in several contexts, including in proteins [211,212]. The experiment using NaSCN contact pairs to probe the charge-transfer reaction in betaine-30 thus represents a particular example of a *transient*, dynamic VSE measurement, where the changes in the electric field produced by the reacting dye induce vibrational frequency shifts of the surrounding solvent shell probes.

Despite the judicious choice of ternary components, the transient VSE signal is still quite weak, and the time scale of the bET reaction is faster than the few picosecond $t_1$ time delay needed to record a 2D-IR spectrum. Because of these practical and fundamental limitations, we probed the reaction using transient DVE spectroscopy (Figure 25), similar to the geminate rebinding study described in Section 4.3. Pump pulses with 5.4 μJ of energy and ~100 fs duration at 580 nm were taken from a non-collinear OPA. The three IR pulses for the echo sequence were incident on the sample, with the relative time delays set at $t_1 = 400$ fs and $t_2 = 0$. The slight $t_1$ delay was chosen to maximise the echo signal, which has a peak shift due to the inhomogeneously broadened CN stretch. The net effect is a better signal-to-noise ratio with a slightly diminished time resolution, but kinetic traces without the time delay showed the same time scales.

It is worthwhile to specify the concentrations of species and the excitation conditions to appreciate how challenging it is to measure these transient DVE spectra. To achieve acceptable IR transmission and visible absorption, the concentrations of betaine-30 (2 mM) and NaSCN (50 mM) were chosen to give 20% IR transmittance and 50% visible transmittance. Based on an estimate of a 200 μm focal diameter for the visible pump and IR probe beams, we can estimate an excitation fraction of 0.1% for the betaine-30 dye molecules ($10^{12}$ photons absorbed/pulse and $10^{15}$ dye molecules in the pumped volume). Hence, only 1 in every 1000 betaine-30 molecules is excited. Since we see a transient signal of roughly $5 \times 10^{-3}$, we conclude that the number of NaSCN contact pairs that respond to the visible excitation of betaine-30 is between 1 and 10, which is consistent with the probes being positioned in the first solvation shell.

A single transient spectrum, shown in Figure 26, at a visible-IR delay of 500 fs indicates a strong bleach at the contact pair absorption around 2060 $cm^{-1}$ and an induced feature centred near 2040 $cm^{-1}$. A dual-Gaussian fit yields a frequency shift of 19 $cm^{-1}$.

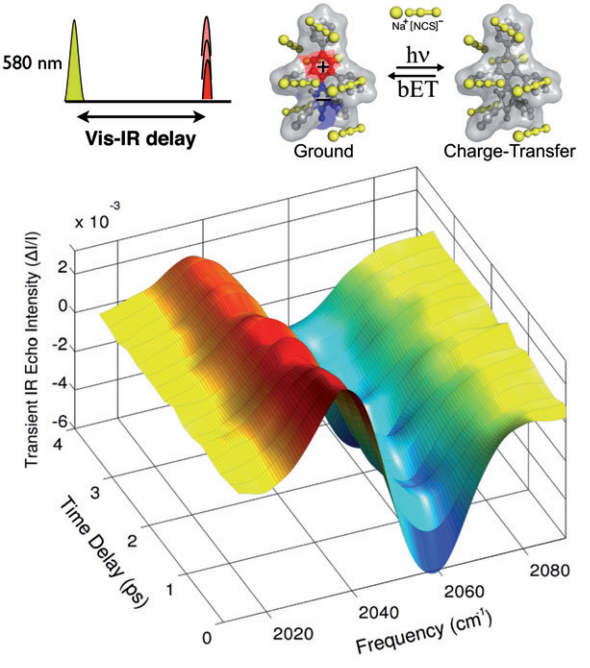


Figure 25. (Colour online) (top) Pulse sequence and cartoon depicting the ultrafast charge-transfer reaction initiated by a 580 nm pulse and probed with DVE using the strong CN stretch of the sodium thiocyanate contact pairs, which act as solvent shell probes. (bottom) Transient DVE spectra show with visible-IR delays ranging from 0 to 4 ps. A clear bleach near 2060 $cm^{-1}$ and an induced signal at 2040 $cm^{-1}$ are signatures of the chemical reaction taking place in the dye, but probed from the perspective of the solvent shell. Adapted with permission from ref. [32]. Copyright 2010 American Chemical Society.

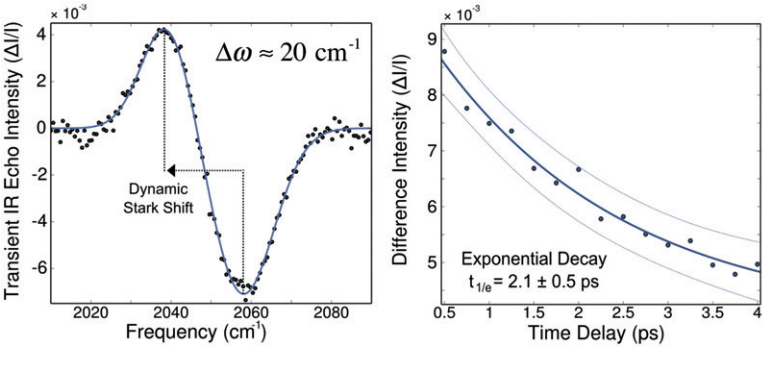


Figure 26. (Colour online) (left) A single transient DVE spectrum recorded at a visible-IR delay of 0.5 ps with a dual-Gaussian fit indicating a 20 $cm^{-1}$ frequency shift. (right) The decay of the induced signal follows a single exponential with a $2.1 \pm 0.5$ ps time constant, which is consistent with other ultrafast studies of betaine-30 bET. Adapted with permission from ref. [32]. Copyright 2010 American Chemical Society.

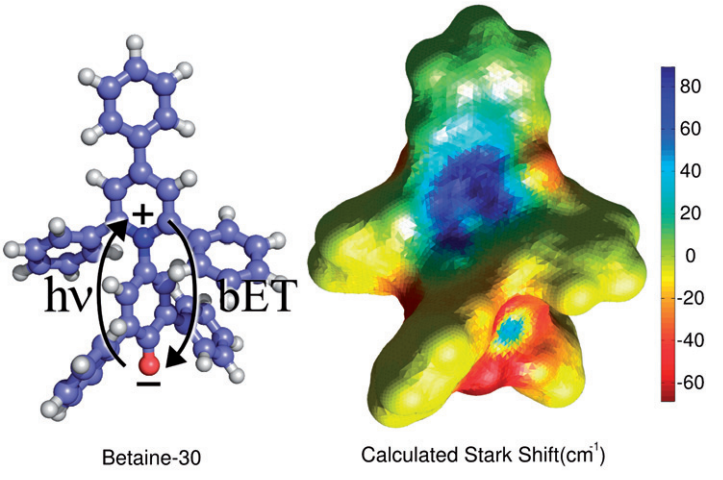


Figure 27. (Colour online) (left) Structure of betaine-30 showing a schematic representation of the photoinduced charge transfer and bET. (right) Computed Stark map using the difference partial charges from the literature [195], evaluated at the points defined by the solvent accessible surface. Adapted with permission from ref. [32]. Copyright 2010 American Chemical Society.

With increased visible-IR delays, the magnitude of the induced signal decreases with a single exponential time constant of $2.1 \pm 0.5$ ps, which agrees with other studies of the bET reaction in betaine-30. To assess whether or not the $19\,cm^{-1}$ frequency shift could be reasonably attributed to a VSE origin, we computed a solvent-accessible (i.e. Conolly) surface on which we determined the maximum possible Stark shift values using the Stark tuning rate for methyl thiocyanate of $0.7\,cm^{-1}/(MV/cm)$. At each point on the surface (Figure 27), we determined the electric field difference between the ground and excited electronic states using the partial charges computed by Mente and Maroncelli [198]. The difference electric field can be mapped to a Stark shift using the tuning rate and the assumption of CN alignment to produce the maximum amplitude shift [209]. That is, the map depicts the most extreme values expected for the spatially heterogeneous Stark shift. The experimentally observed shift of $19\,cm^{-1}$ fits within the estimate provided by this mapping approach.

We would anticipate some degree of alignment within the electrostatic environment created by the charge-separated betaine-30 ground state, and since the Stark effect is directional, it is informative to consider both the effects of laser polarisation and solvent shell alignment on the induced signal. We first consider the laser polarisation, where photoselection should induce an anisotropy in the transient response. Indeed, the magnitude of the induced signal is significantly smaller (40%) when the visible pulse is perpendicularly polarised relative to the three IR pulses. Despite the 40% decrease in induced-DVE signal levels, the time constant of the crossed-polarisation relaxation was determined to be ~2 ps, consistent with the fully polarised case.

Although these polarisation experiments are certainly essential in establishing the preferential alignment of the solvent shell probes, it is actually possible to deduce some degree of alignment simply by the shape of the induced response. For an isotropic

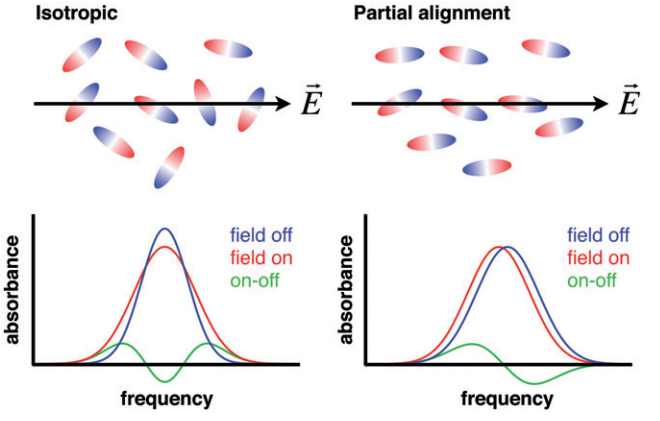


Figure 28. (Colour online) Cartoons depicting Stark difference spectra in the case of isotropic distribution of chromophores (left) and a partially aligned distribution (right). In the dynamic Stark experiment, the electric field is caused by the photoinduced charge-transfer reaction.

distribution of spectroscopic probes in a difference electric field, such as that produced by applying a variable external field using a capacitor arrangement, the difference spectrum resembles a second-derivative shape [212]. This effect can be viewed simplistically as a set of randomly oriented molecules with a Gaussian frequency distribution reflecting, for example, an inhomogeneously broadened band (Figure 28). If an electric field is switched on, the spectral band will necessarily broaden because every projection of the field on the spectroscopically relevant dipole moment is equally probable. The difference between two normalised Gaussians with different widths is a second-derivative shape. If, however, the molecules are partially aligned, some orientations will be preferred, leading to an overall shift of the spectral band and a resulting asymmetric difference spectrum resembling the first derivative. Hence, our observation of an asymmetric-induced DVE spectrum reflects the underlying alignment of the solvent shell probes in the strong electrostatic environment caused by the 17 Debye ground-state dipole moment of betaine-30.

The question remains regarding other processes that can influence the transient IR response that are not directly related to the VSE picture described above. These are the possible thermal contributions and orientational dynamics that accompany the charge transfer and back transfer. Since betaine-30 exhibits little fluorescence, essentially all the energy deposited in the molecule is ultimately released as heat to the surroundings. If the solvent shell probes have a temperature-dependent absorption spectrum, heating might be able to account for the observed DVE shift dynamics. In our measurements, however, we were careful only to consider the first 4 ps of dynamics following the visible pulse. Since it is known that thermalisation of the excess energy within betaine-30 occurs on a 10 ps time scale [194,203,204,208], the sharp 2 ps relaxation of the DVE signal cannot be due to heating of the solvent, which necessarily takes considerably longer than intramolecular vibrational cooling. Indeed, much is already known about heating, so provided the spectral dynamics occur much faster than cooling and thermal energy transport, it is likely a general aspect of dynamic VSE spectroscopy that thermal effects should be avoidable. Orientational dynamics, on the other hand, may certainly be relevant for ultrafast

chemical processes tracked by solvent shell probes. Betaine-30's charge-separated ground state can be thought of as acting to trap the dipolar and polarisable solvent shell molecules, and instantaneously extinguishing the trapping force could allow the solvent shell molecules to freely reorient, only to be snapped back into place by the re-established trap that accompanies the bET process. In the case of NaSCN, the reorientation time is quite slow; even in water, $SCN^-$ exhibits 40 ps orientational relaxation [213]. Near the surface of a large molecule like betaine-30, the orientational diffusion should be even slower. It is very interesting to imagine, however, that if the solvent shell probes could reorient on the time scale of the reaction, there could be a secondary electric field due to the collective reorientation of the polar solvent shell molecules. Such an effect would most likely be observable for slower excited-state reactions, such as the dynamics associated with the formation of twisted intramolecular charge-transfer states.

There are now several transient techniques with demonstrated sensitivity to non-equilibrium solvent shell dynamics. Besides the resonant probe described here, there are approaches that measure transient changes in the non-resonant polarisability response (i.e. Raman) of the solvent in response to electronic excitation. These methods, named alternatively resonant pump third-order Raman spectroscopy [214–216] or resonant pump polarisability response spectroscopy [217–219], use actinic pump modulation of the heterodyne-detected third-order Raman response to deduce the non-equilibrium solvent response. These methods are promising approaches to studying solvation and charge-transfer reaction dynamics from the solvent's perspective [220]. One advantage of the non-resonant probes is their lack of reliance on adding a solvent shell probe. It is not clear, however, how much molecular detail can be obtained from the low-frequency polarisability response, which is notoriously similar for different solvents [221]. Further, the approach described here can be extended to a multidimensional IR probe with straightforward technical improvements, whereas the difficulties of multidimensional Raman spectroscopy have been well documented [92,222,223]. In fact, even in this initial report, we were able to take advantage of the echo-based spectroscopy to alleviate some inhomogeneous broadening, which is inherently impossible using third-order non-resonant probes [224].

## 5. Conclusions and outlook

Chemical reactions are the central focus of chemistry, but they are often challenging to investigate in the condensed phase, particularly with the highest temporal and spectral resolution. Some of this difficulty is inherent to the nature of reactions in complex environments, where disorder and heterogeneity are unavoidable. Perhaps, the ideal experiment would be able to monitor ultrafast reactions of individual molecules, a possibility that has recently moved out of the realm of science fiction [225–228]. If implemented and interpreted properly, however, multidimensional spectroscopy offers many of the rewards promised by single-molecule spectroscopy, such as the ability to separate homogeneous and inhomogeneous broadening, to watch molecules undergo stochastic fluctuations between conformations and to expose non-Gaussian fluctuations. In this review, we have attempted to highlight how 2D-IR spectroscopy is providing new insight into the dynamics of chemical reactions taking place both at equilibrium as well as following a phototrigger. The equilibrium isomerisation of $CO_2(CO)_8$, itself not an

especially significant reaction, is nevertheless a model of low-barrier reactive crossings, enabling a completely new approach to the Kramers problem by focusing on a ground electronic state reaction. The advent of picosecond laser technology in the 1980s spurred a concerted effort to measure and explain dynamical solvent effects on photoisomerisation reactions, leading to several conceptual breakthroughs and novel experimental techniques. Today, 2D-IR chemical exchange and small fluxional organometallic complexes replace time-resolved fluorescence and *trans*-stilbene, but many of the fundamental questions are the same. The next step will be to look beyond Kramers' theory, to the molecularity of the solvent shell, which should be particularly important in complete descriptions of low-barrier enzyme-catalysed reactions. Ultrafast 2D-IR spectroscopy should be able to assess the relative significance of energetics and dynamics in determining enzyme catalysis, particularly in cases where these two somewhat independent contributions can be modified separately by mutations and changes to the surrounding medium (i.e. solvents, membranes, crowders). By using vibrational probes to study ground electronic state dynamics, we are in a position to exploit tremendous improvements in QM/MM simulations to capture both the reaction dynamics and to compute spectra [229–231]. It may turn out that a low-dimensional Langevin-like picture survives, but it will not be a necessary *a priori* assumption. Despite this promise, however, we still require developments in spectroscopic probes with longer lifetimes. We have recently adopted an approach using metal carbonyl labels to probe the protein–water interface [232], and similar advances will be necessary to move beyond the few picosecond lifetimes of the backbone amide-I bands.

Ultrafast spectroscopy is rooted in the quest to capture the dynamics of the fastest transient chemical species. It is, therefore, a natural progression to probe non-equilibrium reactions with 2D-IR spectroscopy. Using several archetypal systems representing the major classes of elementary chemical reaction steps – dissociation, bimolecular association and charge transfer – we have attempted to assemble a set of principles guiding the investigation of transient species with 2D spectroscopy. We and others have only scratched the surface, not yet taking full advantage of the spectral and dynamical information that is routinely extracted from equilibrium 2D-IR spectra. For example, there have been no reports of fluxional motion of photoproducts directly using transient 2D-IR chemical exchange. Though there have been determinations of vibrational energy transfer in photoproducts, these have been for essentially equilibrated photodissociated species long after reaching thermal equilibrium. Line-shape analysis and determination of spectral diffusion are both especially challenging for transient species, primarily due to the large bleach signals that are unavoidable using collinear actinic pump geometries. Perhaps, advances in implementing fully non-collinear transient 2D-IR will alleviate some of these problems. There is little question that in the coming years we will see transient 2D-IR spectroscopy done on surfaces, which are particularly relevant for membrane-bound light-harvesting protein complexes, as well as for interfacial charge transfer central to novel photovoltaic materials and devices. Transient 2D-IR spectroscopy also promises a distinct advantage over transient visible absorption: as long as the vibrational probes remain attached, any electronic state dynamics can be monitored indirectly by the influence on the vibrational frequencies. For transition metal carbonyl, cyanide and thiocyanate complexes, the advantage is due to the simple relationship between metal–ligand charge density, which determines the $\pi$ back bonding, modulating ligand site energies and

their couplings. When probing electronic dynamics using vibrations, there are never any dark states. Advances in quantum chemical calculations of excited electronic state energies and geometries will enable the straightforward extension of approaches used on the ground state to evaluate, for example, the vibrational Hamiltonian of a subset of modes [233]. Though it may currently be impractical to compute all the vibrational modes of a large molecule in one or more electronically excited states, the spectrally isolated metal carbonyl modes, which are weakly coupled to other modes in the molecule, can likely be completely characterised using a low-dimensional potential energy surface. If successful, we will be able to quantitatively model how carbonyl vibrations are able to monitor the intramolecular dynamics of electronically excited photocatalysts and semiconductor sensitisers, just as they have been so useful in revealing ground electronic state solvation dynamics in, for example, alcohols, proteins, water and glasses [78,99,166,232,234].



## Acknowledgements

The authors thank all the graduate students and postdoctorates of the Kubarych group, past and present, who have helped to make this study possible: Matthew Nee, Derek Osborne, John King, Evan Arthur, Aaron White, Josef Dunbar and Laura Kiefer. We have benefited from extremely fruitful collaborations with our colleagues Profs Eitan Geva and Barry Dunietz. This research has been supported by the National Science Foundation (CHE-0748501), the NSF Physics Frontiers Center: Frontiers in Optical, Coherent and Ultrafast Science, the Petroleum Research Fund of the American Chemical Society, the Camille & Henry Dreyfus Foundation, the Rackham Graduate School of the University of Michigan and the Department of Chemistry of the University of Michigan.

## References

[1] S. Woutersen, Y. Mu, G. Stock, and P. Hamm, Chem. Phys. **266**, 137 (2001).
[2] Y. S. Kim and R. M. Hochstrasser, J. Phys. Chem. B **113**, 8231 (2009).
[3] J. Zheng, K. Kwak, and M. D. Fayer, Acc. Chem. Res. **40**, 75 (2007).
[4] J. F. Cahoon, K. R. Sawyer, J. P. Schlegel, and C. B. Harris, Science **319**, 1820 (2008).
[5] J. M. Anna, M. R. Ross, and K. J. Kubarych, J. Phys. Chem. A **113**, 6544 (2009).
[6] M. D. Fayer, Acc. Chem. Res. **45**, 3 (2012).
[7] M. B. Ji, M. Odelius, and K. J. Gaffney, Science **328**, 1003 (2010).
[8] D. E. Rosenfeld, K. Kwak, Z. Gengeliczki, and M. D. Fayer, J. Phys. Chem. B **114**, 2383 (2010).
[9] M. D. Fayer, Annu. Rev. Phys. Chem. **60**, 21 (2009).
[10] Y. S. Kim and R. M. Hochstrasser, J. Phys. Chem. B **111**, 9697 (2007).
[11] Y. S. Kim and R. M. Hochstrasser, Proc. Natl. Acad. Sci. USA **102**, 11 185 (2005).
[12] J. R. Zheng, K. Kwak, J. Asbury, X. Chen, I. R. Piletic, and M. D. Fayer, Science **309**, 1338 (2005).
[13] M. Olschewski, S. Knop, J. Seehusen, J. Lindner, and P. Vohringer, J. Phys. Chem. A **115**, 1210 (2011).
[14] J. R. Zheng and M. D. Fayer, J. Am. Chem. Soc. **129**, 4328 (2007).
[15] J. R. Zheng, K. Kwak, X. Chen, J. B. Asbury, and M. D. Fayer, J. Am. Chem. Soc. **128**, 2977 (2006).
[16] J. R. Zheng, K. W. Kwak, J. Xie, and M. D. Fayer, Science **313**, 1951 (2006).
[17] J. M. Anna and K. J. Kubarych, J. Chem. Phys. **133**, 174 506 (2010).
[18] P. Hamm, J. Helbing, and J. Bredenbeck, Annu. Rev. Phys. Chem. **59**, 291 (2008).

[19] J. Bredenbeck and P. Hamm, Chimia **61**, 45 (2007).
[20] J. Bredenbeck, J. Helbing, C. Kolano, and P. Hamm, ChemPhysChem **8**, 1747 (2007).
[21] E. H. G. Backus, R. Bloem, P. M. Donaldson, J. A. Ihalainen, R. Pfister, B. Paoli, A. Caflisch, and P. Hamm, J. Phys. Chem. B **114**, 3735 (2010).
[22] J. A. Ihalainen, J. Bredenbeck, R. Pfister, J. Helbing, L. Chi, I. H. M. van Stokkum, G. A. Woolley, and P. Hamm, Proc. Natl. Acad. Sci. USA **104**, 5383 (2007).
[23] J. Bredenbeck, J. Helbing, J. R. Kumita, G. A. Woolley, and P. Hamm, Proc. Natl. Acad. Sci. USA **102**, 2379 (2005).
[24] J. Bredenbeck, J. Helbing, R. Behrendt, C. Renner, L. Moroder, J. Wachtveitl, and P. Hamm, J. Phys. Chem. B **107**, 8654 (2003).
[25] C. R. Baiz, R. McCanne, M. J. Nee, and K. J. Kubarych, J. Phys. Chem. A **113**, 8907 (2009).
[26] C. R. Baiz, M. J. Nee, R. McCanne, and K. J. Kubarych, Opt. Lett. **33**, 2533 (2008).
[27] C. Kolano, J. Helbing, M. Kozinski, W. Sander, and P. Hamm, Nature **444**, 469 (2006).
[28] R. Kania, P. W. J. M. Frederix, J. A. Wright, R. V. Ulijn, C. J. Pickett, and N. T. Hunt, J. Chem. Phys. **136**, 044 521 (2012).
[29] A. I. Stewart, J. A. Wright, G. M. Greetham, S. Kaziannis, S. Santabarbara, M. Towrie, A. W. Parker, C. J. Pickett, and N. T. Hunt, Inorg. Chem. **49**, 9563 (2010).
[30] S. Kaziannis, S. Santabarbara, J. A. Wright, G. M. Greetham, M. Towrie, A. W. Parker, C. J. Pickett, and N. T. Hunt, J. Phys. Chem. B **114**, 15 370 (2010).
[31] C. R. Baiz, R. McCanne, and K. J. Kubarych, J. Am. Chem. Soc. **131**, 13 590 (2009).
[32] C. R. Baiz and K. J. Kubarych, J. Am. Chem. Soc. **132**, 12 784 (2010).
[33] H. S. Chung, M. Khalil, A. W. Smith, and A. Tokmakoff, Rev. Sci. Instrum. **78**, 063 101 (2007).
[34] D. Chung, Z. Ganim, K. C. Jones, and T. Tokmakoff, Proc. Natl. Acad. Sci. USA **104**, 14 237 (2007).
[35] M. Cho, Chem. Rev. **108**, 1331 (2008).
[36] D. M. Jonas, Annu. Rev. Phys. Chem. **54**, 425 (2003).
[37] M. Khalil, N. Demirdoven, and A. Tokmakoff, J. Phys. Chem. A **107**, 5258 (2003).
[38] J. Zheng, K. Kwak, and M. D. Fayer, Acc. Chem. Res. **40**, 75 (2007).
[39] F. Fournier, R. Guo, E. M. Gardner, P. M. Donaldson, C. Loeffeld, I. R. Gould, K. R. Willison, and D. R. Klug, Acc. Chem. Res. **42**, 1322 (2009).
[40] T. Elsaesser, Acc. Chem. Res. **42**, 1220 (2009).
[41] T. L. C. Jansen and J. Knoester, Acc. Chem. Res. **42**, 1405 (2009).
[42] R. J. D. Miller, A. Paarmann, and V. I. Prokhorenko, Acc. Chem. Res. **42**, 1442 (2009).
[43] I. V. Rubtsov, Acc. Chem. Res. **42**, 1385 (2009).
[44] W. Zhuang, T. Hayashi, and S. Mukamel, Angew. Chem. Int. Ed. **48**, 3750 (2009).
[45] J. P. Ogilvie and K. J. Kubarych, Adv. At. Mol. Opt. Phys. **57**, 249 (2009).
[46] S. Park, K. Kwak, and M. D. Fayer, Laser Phys. Lett. **4**, 704 (2007).
[47] M. Cho, *Two-dimensional Optical Spectroscopy* (CRC Press, Boca Raton, FL, 2009).
[48] P. Hamm and M. T. Zanni, *Concepts and Methods of 2D Infrared Spectroscopy* (Cambridge University Press, New York, 2011).
[49] R. A. Kaindl, M. Wurm, K. Reimann, P. Hamm, A. M. Weiner, and M. Woerner, J. Opt. Soc. Am. B: Opt. Phys. **17**, 2086 (2000).
[50] P. Hamm, M. Lim, W. F. DeGrado, and R. M. Hochstrasser, Proc. Natl. Acad. Sci. USA **96**, 2036 (1999).
[51] A. I. Stewart, I. P. Clark, M. Towrie, S. K. Ibrahim, A. W. Parker, C. J. Pickett, and N. T. Hunt, J. Phys. Chem. B **112**, 10 023 (2008).
[52] D. B. Strasfeld, S. H. Shim, and M. T. Zanni, Adv. Chem. Phys. **141**, 1 (2009).
[53] H. T. Bian, J. B. Li, X. W. Wen, Z. G. Sun, J. A. Song, W. Zhuang, and J. R. Zheng, J. Phys. Chem. A **115**, 3357 (2011).
[54] V. Cervetto, J. Helbing, J. Bredenbeck, and P. Hamm, J. Chem. Phys. **121**, 5935 (2004).

[55] M. C. Asplund, M. T. Zanni, and R. M. Hochstrasser, Proc. Natl. Acad. Sci. USA **97**, 8219 (2000).
[56] I. V. Rubtsov, K. Kumar, and R. M. Hochstrasser, Chem. Phys. Lett. **402**, 439 (2005).
[57] I. V. Rubtsov, J. Wang, and R. M. Hochstrasser, J. Chem. Phys. **118**, 7733 (2003).
[58] I. V. Rubtsov, J. P. Wang, and R. M. Hochstrasser, Proc. Natl. Acad. Sci. USA **100**, 5601 (2003).
[59] J. P. Likforman, M. Joffre, and V. ThierryMieg, Opt. Lett. **22**, 1104 (1997).
[60] M. F. Emde, W. P. deBoeij, M. S. Pshenichnikov, and D. A. Wiersma, Opt. Lett. **22**, 1338 (1997).
[61] M. L. Cowan, J. P. Ogilvie, and R. J. D. Miller, Chem. Phys. Lett. **386**, 184 (2004).
[62] J. M. Anna, M. J. Nee, C. R. Baiz, R. McCanne, and K. J. Kubarych, J. Opt. Soc. Am. B: Opt. Phys. **27**, 382 (2010).
[63] L. P. DeFlores, R. A. Nicodemus, and A. Tokmakoff, Opt. Lett. **32**, 2966 (2007).
[64] P. E. Tekavec, J. A. Myers, K. L. M. Lewis, and J. P. Ogilvie, Opt. Lett. **34**, 1390 (2009).
[65] J. A. Myers, K. L. M. Lewis, P. F. Tekavec, and J. P. Ogilvie, Opt. Express **16**, 17 420 (2008).
[66] S. H. Shim, D. B. Strasfeld, Y. L. Ling, and M. T. Zanni, Proc. Natl. Acad. Sci. USA **104**, 14 197 (2007).
[67] E. M. Grumstrup, S. H. Shim, M. A. Montgomery, N. H. Damrauer, and M. T. Zanni, Opt. Express **15**, 16 681 (2007).
[68] C. R. Baiz and K. J. Kubarych, Opt. Lett. **36**, 187 (2011).
[69] K. F. Lee, P. Nuernberger, A. Bonvalet, and M. Joffre, Opt. Express **17**, 18 738 (2009).
[70] K. F. Lee, K. J. Kubarych, A. Bonvalet, and M. Joffre, J. Opt. Soc. Am. B: Opt. Phys. **25**, A54 (2008).
[71] M. J. Nee, R. McCanne, K. J. Kubarych, and M. Joffre, Opt. Lett. **32**, 713 (2007).
[72] K. J. Kubarych, M. Joffre, A. Moore, N. Belabas, and D. M. Jonas, Opt. Lett. **30**, 1228 (2005).
[73] J. Zhu, T. Mathes, A. D. Stahl, J. T. M. Kennis, and M. L. Groot, Opt. Express **20**, 10 562 (2012).
[74] S. Mukamel, *Principles of Nonlinear Optical Spectroscopy* (Oxford University Press, New York, 1995).
[75] J. B. Asbury, T. Steinel, and M. D. Fayer, Chem. Phys. Lett. **381**, 139 (2003).
[76] J. M. Anna, J. T. King, and K. J. Kubarych, Inorg. Chem. **50**, 9273 (2011).
[77] Z. W. Lin and I. V. Rubtsov, Proc. Natl. Acad. Sci. USA **109**, 1413 (2012).
[78] J. T. King, J. M. Anna, and K. J. Kubarych, Phys. Chem. Chem. Phys. **13**, 5579 (2011).
[79] R. Kania, A. I. Stewart, I. P. Clark, G. M. Greetham, A. W. Parker, M. Towrie, and N. T. Hunt, Phys. Chem. Chem. Phys. **12**, 1051 (2010).
[80] K. Ramasesha, S. T. Roberts, R. A. Nicodemus, A. Mandal, and A. Tokmakoff, J. Chem. Phys. **135**, 054 509 (2011).
[81] F. Perakis and P. Hamm, J. Phys. Chem. B **115**, 5289 (2011).
[82] G. Stirnemann and D. Laage, J. Phys. Chem. Lett. **1**, 1511 (2010).
[83] K. J. Gaffney, P. H. Davis, I. R. Piletic, N. E. Levinger, and M. A. Fayer, J. Phys. Chem. A **106**, 12 012 (2002).
[84] K. J. Gaffney, I. R. Piletic, and M. D. Fayer, J. Chem. Phys. **118**, 2270 (2003).
[85] K. J. Gaffney, I. R. Piletic, and M. D. Fayer, J. Phys. Chem. A **106**, 9428 (2002).
[86] K. Kwac and E. Geva, J. Phys. Chem. B **116**, 2856 (2012).
[87] K. Kwac and E. Geva, J. Phys. Chem. B **115**, 9184 (2011).
[88] M. Khalil, N. Demirdoven, and A. Tokmakoff, Phys. Rev. Lett. **90**, 047 401 (2003).
[89] S. T. Roberts, J. J. Loparo, and A. Tokmakoff, J. Chem. Phys. **125**, 084 502 (2006).
[90] B. M. Ladanyi and R. M. Stratt, J. Phys. Chem. **99**, 2502 (1995).
[91] T. L. C. Jansen and J. Knoester, J. Chem. Phys. **127**, 234 502 (2007).
[92] K. J. Kubarych, C. J. Milne, and R. J. D. Miller, Int. Rev. Phys. Chem. **22**, 497 (2003).
[93] S. Garrett-Roe, F. Perakis, F. Rao, and P. Hamm, J. Phys. Chem. B **115**, 6976 (2011).

[94] F. Ding and M. T. Zanni, Chem. Phys. **341**, 95 (2007).
[95] J. Bredenbeck, J. Helbing, and P. Hamm, J. Am. Chem. Soc. **126**, 990 (2004).
[96] W. Xiong, J. E. Laaser, P. Paoprasert, R. A. Franking, R. J. Hamers, P. Gopalan, and M. T. Zanni, J. Am. Chem. Soc. **131**, 18040 (2009).
[97] C. R. Baiz, R. McCanne, and K. J. Kubarych, Appl. Spectrosc. **64**, 1037 (2010).
[98] K. C. Jones, Z. Ganim, and A. Tokmakoff, J. Phys. Chem. A **113**, 14 060 (2009).
[99] J. T. King, M. R. Ross, and K. J. Kubarych, Phys. Rev. Lett. **108**, 157 401 (2012).
[100] S. M. Arrivo, V. D. Kleiman, W. T. Grubbs, T. P. Dougherty, and E. J. Heilweil, Laser Chem. **19**, 1 (1999).
[101] S. M. Arrivo and E. J. Heilweil, J. Phys. Chem. **100**, 11 975 (1996).
[102] S. Woutersen, Y. Mu, G. Stock, and P. Hamm, Chem. Phys. **266**, 137 (2001).
[103] D. Chandler, *Introduction to Modern Statistical Mechanics* (Oxford University Press, New York, 1987).
[104] N. E. Levinger, P. H. Davis, P. K. Behera, D. J. Myers, C. Stromberg, and M. D. Fayer, J. Chem. Phys. **118**, 1312 (2003).
[105] C. L. Perrin and T. J. Dwyer, Chem. Rev. **90**, 935 (1990).
[106] M. D. Fayer, D. E. Moilanen, D. Wong, D. E. Rosenfeld, E. E. Fenn, and S. Park, Acc. Chem. Res. **42**, 1210 (2009).
[107] D. E. Moilanen, D. Wong, D. E. Rosenfeld, E. E. Fenn, and M. D. Fayer, Proc. Natl. Acad. Sci. USA **106**, 375 (2009).
[108] D. E. Moilanen, E. E. Fenn, D. Wong, and M. D. Fayer, J. Am. Chem. Soc. **131**, 8318 (2009).
[109] D. E. Moilanen, E. E. Fenn, D. Wong, and M. D. Fayer, J. Phys. Chem. B **113**, 8560 (2009).
[110] D. E. Moilanen, E. E. Fenn, D. Wong, and M. D. Fayer, J. Chem. Phys. **131**, 014 704 (2009).
[111] S. Bagchi, D. G. Thorpe, I. F. Thorpe, G. A. Voth, and M. D. Fayer, J. Phys. Chem. B **114**, 17 187 (2010).
[112] C. H. Kuo and R. M. Hochstrasser, Chem. Phys. **341**, 21 (2007).
[113] C. H. Kuo, D. Y. Vorobyev, J. X. Chen, and R. M. Hochstrasser, J. Phys. Chem. B **111**, 14 028 (2007).
[114] J. H. Ha, Y. S. Kim, and R. M. Hochstrasser, J. Chem. Phys. **124**, 064 508 (2006).
[115] Y. S. Kim and R. M. Hochstrasser, J. Phys. Chem. B **110**, 8531 (2006).
[116] A. Ghosh, J. Qiu, W. F. DeGrado, and R. M. Hochstrasser, Proc. Natl. Acad. Sci. USA **108**, 6115 (2011).
[117] R. S. Berry, J. Chem. Phys. **32**, 933 (1960).
[118] F. A. Cotton, J. Organomet. Chem. **100**, 29 (1975).
[119] R. Bramley, R. S. Nyholm, and B. N. Figgis, Trans. Faraday Soc. **58**, 1893 (1962).
[120] P. Hanggi, P. Talkner, and M. Borkovec, Rev. Mod. Phys. **62**, 251 (1990).
[121] P. Talkner and P. Hanggi, *New Trends in Kramers' Reaction Rate Theory* (Kluwer Academic Publishers, Netherlands, 1995).
[122] E. Pollak, J. Chem. Phys. **103**, 973 (1995).
[123] A. M. Berezhkovskii, A. M. Frishman, and E. Pollak, J. Chem. Phys. **101**, 4778 (1994).
[124] D. G. Truhlar and B. C. Garrett, Annu. Rev. Phys. Chem. **35**, 159 (1984).
[125] D. G. Truhlar and B. C. Garrett, Acc. Chem. Res. **13**, 440 (1980).
[126] G. R. Fleming, S. H. Courtney, and M. W. Balk, J. Stat. Phys. **42**, 83 (1986).
[127] M. I. Sluch, M. M. Somoza, and M. A. Berg, J. Phys. Chem. B **106**, 7385 (2002).
[128] M. Y. Lee, J. N. Haseltine, A. B. Smith, and R. M. Hochstrasser, J. Am. Chem. Soc. **111**, 5044 (1989).
[129] R. F. Grote and J. T. Hynes, J. Chem. Phys. **73**, 2715 (1980).
[130] A. M. Berezhkovskii, E. Pollak, and V. Y. Zitserman, J. Chem. Phys. **97**, 2422 (1992).
[131] A. Ansari, C. M. Jones, E. R. Henry, J. Hofrichter, and W. A. Eaton, Science **256**, 1796 (1992).
[132] R. Tannenbaum and G. Bor, J. Organomet. Chem. **586**, 18 (1999).
[133] Y. K. Chung, Coord. Chem. Rev. **188**, 297 (1999).

[134] R. L. Sweany and T. L. Brown, Inorg. Chem. **16**, 415 (1977).
[135] J. P. Kenny, R. B. King, and H. F. Schaefer, Inorg. Chem. **40**, 900 (2001).
[136] G. Aullon and S. Alvarez, Eur. J. Inorg. Chem. **2001**, 3031 (2001).
[137] M. J. Nee, C. R. Baiz, J. M. Anna, R. McCanne, and K. J. Kubarych, J. Chem. Phys. **129**, 084503 (2008).
[138] C. R. Baiz, K. J. Kubarych, and E. Geva, J. Phys. Chem. B **115**, 5322 (2011).
[139] O. Golonzka, M. Khalil, N. Demirdoven, and A. Tokmakoff, J. Chem. Phys. **115**, 10 814 (2001).
[140] A. M. Moran, J. Dreyer, and S. Mukamel, J. Chem. Phys. **118**, 1347 (2003).
[141] A. M. Brearley, S. R. Flom, V. Nagarajan, and P. F. Barbara, J. Phys. Chem. **90**, 2092 (1986).
[142] S. R. Flom, V. Nagarajan, and P. F. Barbara, J. Phys. Chem. **90**, 2085 (1986).
[143] P. S. Hubbard, Phys. Rev. **131**, 1155 (1963).
[144] W. W. Cleland and M. M. Kreevoy, Science **264**, 1887 (1994).
[145] S. Dutta, R. J. Cook, J. C. D. Houtman, A. Kohen, and C. M. Cheatum, Anal. Biochem. **407**, 241 (2010).
[146] S. E. Hill, J. N. Bandaria, M. Fox, E. Vanderah, A. Kohen, and C. M. Cheatum, J. Phys. Chem. B **113**, 11 505 (2009).
[147] J. N. Bandaria, S. Dutta, S. E. Hill, A. Kohen, and C. M. Cheatum, J. Am. Chem. Soc. **130**, 22 (2008).
[148] W. Min, B. P. English, G. B. Luo, B. J. Cherayil, S. C. Kou, and X. S. Xie, Acc. Chem. Res. **38**, 923 (2005).
[149] J. Bredenbeck, J. Helbing, A. Sieg, T. Schrader, W. Zinth, C. Renner, R. Behrendt, L. Moroder, J. Wachtveitl, and P. Hamm, Proc. Natl. Acad. Sci. USA **100**, 6452 (2003).
[150] J. Bredenbeck, J. Helbing, K. Nienhaus, G. U. Nienhaus, and P. Hamm, Proc. Natl. Acad. Sci. USA **104**, 14 243 (2007).
[151] V. Cervetto, P. Hamm, and J. Helbing, J. Phys. Chem. B **112**, 8398 (2008).
[152] H. S. Chung, Z. Ganim, K. C. Jones, and A. Tokmakoff, Proc. Natl. Acad. Sci. USA **104**, 14 237 (2007).
[153] N. V. Vitanov, T. Halfmann, B. W. Shore, and K. Bergmann, Annu. Rev. Phys. Chem. **52**, 763 (2001).
[154] P. M. Donaldosn, H. Strzalka, and P. Hamm, Opt. Express **20**, 12 761 (2012).
[155] J. Helbing, H. Bregy, J. Bredenbeck, R. Pfister, P. Hamm, R. Huber, J. Wachtveitl, L. de Vico, and M. Olivucci, J. Am. Chem. Soc. **126**, 8823 (2004).
[156] J. Bredenbeck, J. Helbing, K. Nienhaus, G. U. Nienhaus, and P. Hamm, Ultrafast Phenomena XV **88**, 377 (2007).
[157] K. C. Jones, Z. Ganim, C. S. Peng, and A. Tokmakoff, J. Opt. Soc. Am. B: Opt. Phys. **29**, 118 (2012).
[158] D. A. Steinhurst, A. P. Baronavski, and J. C. Owrutsky, Chem. Phys. Lett. **361**, 513 (2002).
[159] J. Helbing, M. Devereux, K. Nienhaus, G. U. Nienhaus, P. Hamm, and M. Meuwly, J. Phys. Chem. A **116**, 2620 (2012).
[160] S. Velate, E. O. Danilov, and M. A. J. Rodgers, J. Phys. Chem. A **109**, 8969 (2005).
[161] P. Hamm, S. Ohline, M. Zurek, and T. Roschinger, Laser Chem. **19**, 45 (1999).
[162] D. A. Prinslow and V. Vaida, J. Am. Chem. Soc. **109**, 5097 (1987).
[163] A. Veillard and M. M. Rohmer, Int. J. Quantum Chem. **42**, 965 (1992).
[164] J. Z. Zhang and C. B. Harris, J. Chem. Phys. **95**, 4024 (1991).
[165] L. J. Rothberg, N. J. Cooper, K. S. Peters, and V. Vaida, J. Am. Chem. Soc. **104**, 3536 (1982).
[166] J. T. King, C. R. Baiz, and K. J. Kubarych, J. Phys. Chem. A **114**, 10 590 (2010).
[167] C. R. Baiz, P. L. McRobbie, J. M. Anna, E. Geva, and K. J. Kubarych, Acc. Chem. Res. **42**, 1395 (2009).
[168] C. R. Baiz, P. L. McRobbie, N. K. Preketes, K. J. Kubarych, and E. Geva, J. Phys. Chem. A **113**, 9617 (2009).

[169] T. P. Dougherty and E. J. Heilweil, Chem. Phys. Lett. **227**, 19 (1994).
[170] H. S. Eom, S. C. Jeoung, D. Kim, J. H. Ha, and Y. R. Kim, J. Phys. Chem. A **101**, 3661 (1997).
[171] E. Rabinowitch and W. C. Wood, Trans. Faraday Soc. **32**, 1381 (1936).
[172] J. Franck and E. Rabinowitch, Trans. Faraday Soc. **30**, 120 (1934).
[173] A. B. Oelkers, E. J. Schutte, and D. R. Tyler, Photochem. Photobiol. Sci. **7**, 228 (2008).
[174] A. B. Oelkers and D. R. Tyler, Photochem. Photobiol. Sci. **7**, 1386 (2008).
[175] A. B. Oelkers, L. F. Scatena, and D. R. Tyler, J. Phys. Chem. A **111**, 5353 (2007).
[176] J. L. Male, M. G. Yoon, A. G. Glenn, T. J. R. Weakley, and D. R. Tyler, Macromolecules **32**, 3898 (1999).
[177] J. L. Male, B. E. Lindfors, K. J. Covert, and D. R. Tyler, J. Am. Chem. Soc. **120**, 13 176 (1998).
[178] B. E. Lindfors, J. L. Male, K. J. Covert, and D. R. Tyler, Chem. Commun. 1687 (1997).
[179] J. L. Male, B. E. Lindfors, K. J. Covert, and D. R. Tyler, Macromolecules **30**, 6404 (1997).
[180] B. E. Lindfors, G. F. Nieckarz, D. R. Tyler, and A. G. Glenn, J. Photochem. Photobiol. A **94**, 101 (1996).
[181] J. Peters, M. W. George, and J. J. Turner, Organometallics **14**, 1503 (1995).
[182] C. R. Baiz, R. McCanne, and K. J. Kubarych, *Structurally-sensitive Rebinding Dynamics of Solvent-caged Radical Pairs: Exploring the Viscosity Dependence* (Oxford University Press, New York, 2011).
[183] M. L. Horng, J. A. Gardecki, A. Papazyan, and M. Maroncelli, J. Phys. Chem. **99**, 17 311 (1995).
[184] T. Q. Lian, Y. Kholodenko, and R. M. Hochstrasser, J. Phys. Chem. **99**, 2546 (1995).
[185] C. Reichardt, Chem. Rev. **94**, 2319 (1994).
[186] T. Ishida and P. J. Rossky, J. Phys. Chem. B **112**, 11 353 (2008).
[187] T. Ishida and P. J. Rossky, J. Phys. Chem. A **105**, 558 (2001).
[188] S. Nishiyama, S. Aikawa, Y. Yoshida, and M. Tajima, Mol. Cryst. Liq. Cryst. **462**, 257 (2007).
[189] H. Kim, H. Hwang, and P. J. Rossky, J. Phys. Chem. A **110**, 11 223 (2006).
[190] H. Hwang and P. J. Rossky, J. Phys. Chem. B **108**, 6723 (2004).
[191] H. Hwang and P. J. Rossky, J. Phys. Chem. A **108**, 2607 (2004).
[192] X. H. Zhao, J. A. Burt, and J. L. McHale, J. Chem. Phys. **121**, 11 195 (2004).
[193] X. H. Zhao, F. J. Knorr, and J. L. McHale, Chem. Phys. Lett. **356**, 214 (2002).
[194] S. A. Kovalenko, N. Eilers-Konig, T. A. Senyushkina, and N. P. Ernsting, J. Phys. Chem. A **105**, 4834 (2001).
[195] S. Hogiu, J. Dreyer, M. Pfeiffer, K. W. Brzezinka, and W. Werncke, J. Raman Spectrosc. **31**, 797 (2000).
[196] S. Hogiu, W. Werncke, M. Pfeiffer, J. Dreyer, and T. Elsaesser, J. Chem. Phys. **113**, 1587 (2000).
[197] J. Lobaugh and P. J. Rossky, J. Phys. Chem. A **104**, 899 (2000).
[198] S. R. Mente and M. Maroncelli, J. Phys. Chem. B **103**, 7704 (1999).
[199] R. Scholz, M. Darwish, and M. Schreiber, J. Lumin **76–77**, 404 (1998).
[200] Y. P. Zong and J. L. McHale, J. Chem. Phys. **106**, 4963 (1997).
[201] C. Fuchs and M. Schreiber, J. Chem. Phys. **105**, 1023 (1996).
[202] P. J. Reid and P. F. Barbara, J. Phys. Chem. **99**, 3554 (1995).
[203] G. C. Walker, E. Akesson, A. E. Johnson, N. E. Levinger, and P. F. Barbara, J. Phys. Chem. **96**, 3728 (1992).
[204] E. Akesson, G. C. Walker, and P. F. Barbara, J. Chem. Phys. **95**, 4188 (1991).
[205] M. C. Beard, G. M. Turner, and C. A. Schmuttenmaer, in *Liquid Dynamics: Experiment, Simulation, and Theory (ACS Symposium Series)*, edited by J. T. Fourkas (ACS, Washington, D.C., 2002), Vol. 820, p. 44.
[206] P. Firman, M. Xu, E. M. Eyring, and S. Petrucci, J. Phys. Chem. **96**, 8631 (1992).
[207] M. C. Beard, G. M. Turner, and C. A. Schmuttenmaer, J. Phys. Chem. A **106**, 878 (2002).

[208] N. E. Levinger, A. E. Johnson, G. C. Walker, and P. F. Barbara, Chem. Phys. Lett. **196**, 159 (1992).
[209] S. H. Brewer and S. Franzen, J. Chem. Phys. **119**, 851 (2003).
[210] E. S. Park, S. S. Andrews, R. B. Hu, and S. G. Boxer, J. Phys. Chem. B **103**, 9813 (1999).
[211] S. Bagchi, S. G. Boxer, and M. D. Fayer, J. Phys. Chem. B **116**, 4034 (2012).
[212] S. G. Boxer, J. Phys. Chem. B **113**, 2972 (2009).
[213] M. B. Ji and K. J. Gaffney, J. Chem. Phys. **134**, 044 516 (2011).
[214] S. J. Schmidtke, D. F. Underwood, and D. A. Blank, J. Phys. Chem. A **109**, 7033 (2005).
[215] D. F. Underwood and D. A. Blank, J. Phys. Chem. A **109**, 3295 (2005).
[216] D. F. Underwood and D. A. Blank, J. Phys. Chem. A **107**, 956 (2003).
[217] M. A. Hershberger, A. M. Moran, and N. F. Scherer, J. Phys. Chem. B **115**, 5617 (2011).
[218] A. M. Moran, S. Park, and N. F. Scherer, Chem. Phys. **341**, 344 (2007).
[219] A. M. Moran, R. A. Nome, and N. F. Scherer, J. Chem. Phys. **127**, 184 505 (2007).
[220] X. Sun and R. M. Stratt, Phys. Chem. Chem. Phys. **14**, 6320 (2012).
[221] Q. Zhong and J. T. Fourkas, J. Phys. Chem. B **112**, 15 529 (2008).
[222] K. J. Kubarych, C. J. Milne, S. Lin, V. Astinov, and R. J. D. Miller, J. Chem. Phys. **116**, 2016 (2002).
[223] K. J. Kubarych, C. J. Milne, and R. J. D. Miller, Chem. Phys. Lett. **369**, 635 (2003).
[224] R. F. Loring and S. Mukamel, J. Chem. Phys. **83**, 2116 (1985).
[225] D. Brinks, R. Hildner, F. D. Stefani, and N. F. van Hulst, Faraday Discuss. **153**, 51 (2011).
[226] R. Hildner, D. Brinks, F. D. Stefani, and N. F. van Hulst, Phys. Chem. Chem. Phys. **13**, 1888 (2011).
[227] R. Hildner, D. Brinks, and N. F. van Hulst, Nat. Phys. **7**, 172 (2011).
[228] D. Brinks, F. D. Stefani, F. Kulzer, R. Hildner, T. H. Taminiau, Y. Avlasevich, K. Mullen, and N. F. v. a. n. Hulst, Nature **465**, 905 (2010).
[229] I. S. Ufimtsev, N. Luehr, and T. J. Martinez, J. Phys. Chem. Lett. **2**, 1789 (2011).
[230] I. S. Ufimtsev and T. J. Martinez, J. Chem. Theory Comput. **5**, 2619 (2009).
[231] I. S. Ufimtsev and T. J. Martinez, J. Chem. Theory Comput. **4**, 222 (2008).
[232] J. T. King, E. J. Arthur, C. L. Brooks, and K. J. Kubarych, J. Phys. Chem. B **116**, 5604 (2012).
[233] C. R. Baiz, K. J. Kubarych, E. Geva, and E. L. Sibert, J. Phys. Chem. A **115**, 5354 (2011).
[234] J. T. King, M. R. Ross, and K. J. Kubarych, J. Phys. Chem. B **116**, 3754 (2012).